Journal of Manufacturing Processes 121 (2024) 150–171

Contents lists available at ScienceDirect

Journal of Manufacturing Processes

journal homepage: www.elsevier.com/locate/manpro

Evaluation of high-frequency roughness measurement errors for composite and ceramic surfaces after machining

Przemysław Podulka [a,*], Wojciech Macek [b], Mirosław Szala [c], Andrzej Kubit [a], Kinkar Chandra Das [d], Grzegorz Królczyk [e]

[a] Faculty of Mechanical Engineering and Aeronautics, Rzeszow University of Technology, Powstancow Warszawy 12, 35-959 Rzeszów, Poland
[b] Faculty of Mechanical Engineering and Ship Technology, Gdańsk University of Technology, Narutowicza 11/12, 80-233 Gdańsk, Poland
[c] Department of Materials Engineering, Faculty of Mechanical Engineering, Lublin University of Technology, Nadbystrzycka 36D, 20-618 Lublin, Poland
[d] Department of Mathematics, Sungkyunkwan University, Suwon 16419, Republic of Korea
[e] Faculty of Mechanical Engineering, Opole University of Technology, 45-271 Opole, Mikolajczyka 5, Poland

ARTICLE INFO

Keywords:
Surface topography
Roughness
Measurement noise
Ceramics
Composites
Surface machining
Honing
Milling
Grinding

ABSTRACT

Precise characterisation of surface topography is of the greatest importance since many factors directly affect the accuracy of the whole measurement process. In this paper, the variety of surface topographies from machined composite and ceramic workpieces was studied with a special emphasis on the measurement results. Surfaces were subjected to the ground diamond, honing and milling processes. Measurement results were analysed in terms of the application of the procedure for the removal of the high-frequency noise. Bandwidth characteristics were supported by the studies of autocorrelation and power spectral functions. It was found, that examination of noisy data, especially its isotropic properties, is crucial in the enhancement of the noise-removal methods. The proposed procedure was validated through direction and profile characterisation. The spline filtering technique with a 7.5 μm cut-off was encouraged against other generally used filtering techniques for the reduction of high-frequency measurement noise considering the study based on the power spectral, autocorrelation and direction functions. The proposed methodology was validated by comparing it to the averaged results of 3 time repeated measurements of the composite and ceramic surfaces after machining. The main advantage of the proposal is reducing the time of data processing due to the fast and easy-to-implement usage of general surface topography analysis functions, available in the commercial software of the measuring instrument.

1. Introduction

Comprehensive studies of surface topography may substantially contribute to many reports on the materials' properties, including the nanoscale nature of the surface undulations [1]. Even historically, Sherrington et al. [2] indicated, that all of the machining processes produce some characteristic topographic features on the specimens' surfaces, that could be improperly identified during surface topography considerations. Tribologically, Chowdhury et al. [3] marked, that many patterns are followed by the sequence of topographic changes in terms of roughness characterisation. Even proceeding with surface topography evolution, analysis and prediction of roughness play a fundamental role in many popular surface finishing methods [4], including laser machining.

Generally, the surface topography received from the machined part measurement can be classified as critical for component performance in terms of its precision or ultra-precision [5]. Waikar et al. [6] represented 'extreme', gentle and abusive machining conditions on turned and ground specimens. Wojciechowski et al. [7] proved the limitless potential of surface topography measurements in the identification of tram wheel tyre wear. The ballistics signatures, which are geometrical micro-topographies by their nature, were directly correlated with the topography as well [8]. Benardos et al. [9] presented a wide review of the advantages and disadvantages of the various practices applied for surface roughness prediction. Szwajka et al. [10] presented an artificial neural network (ANN) study on wood-based composite surface roughness, that is significant in a medium-density fiberboard milling process analysis. The precise determination of the surface roughness parameters

* Corresponding author.
E-mail addresses: p.podulka@prz.edu.pl (P. Podulka), wojciech.macek@pg.edu.pl (W. Macek), m.szala@pollub.pl (M. Szala), a.kubit@prz.edu.pl (A. Kubit), g.krolczyk@po.opole.pl (G. Królczyk).

https://doi.org/10.1016/j.jmapro.2024.05.032
Received 8 January 2024; Received in revised form 8 May 2024; Accepted 11 May 2024
Available online 20 May 2024

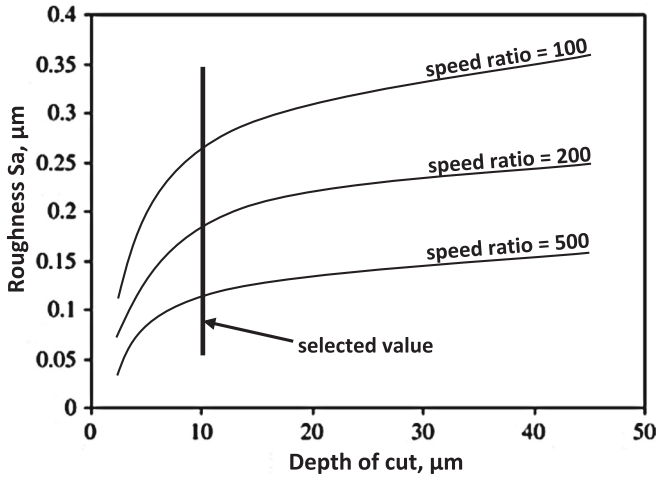

Fig. 1. The relation of surface roughness and depth of cut for three different rotation speeds during grinding (based on [63]).

after machining can be severely disrupted by the errors occurred during the measurement process. One should highlight, that surface topography is often measured by devices roughly divided into two groups, determined by the measurement method. The first, are originally dedicated and widely applied tactile techniques. The stylus-type profilometers are widely known as those giving actual information about the surface profile. The width of the stylus tip must be, however, smaller than the lateral size of the surface irregularities [11]. Except for sufficient accuracy, the contact techniques suffer from severe disadvantages, for example, stylus measurement limitations by the tip radius and they are time-consuming [12].

Thus, non-contact techniques, that use an optical profiler with a self-reference laser concerning stylus instruments, are lately of great interest. Especially when displacement measurement improvements are demanded [13]. As a consequence, area-based light scattering for roughness assessment using machine vision methods partially overcame the low-speed measurement issues for turned parts [14]. Noteworthy advancement was acknowledged by White Light Interferometry (WLI), which has been proven to be an effective technique for surface topography determination [15]. Through the years, this method has been designated as resolving many measurement problems, especially for measuring the inner surface topography [16]. Viotti et al. [17] confirmed the ability of WLI to measure a sizeable portion of points from the surface data evaluated. Wu et al. [18] studied the turned surface topographies with in situ measurements and found them suitable for the analysis of tool posture, surface geometry and roughness evaluation. An interesting approach was also presented by Li et al. [19], who calibrated an ultra-precision turning machine with on-machine measurement systems for interferometric surface metrology purposes.

Except large number of WLI advantages for the roughness measurement application, limitations of this technique were also exposed in the literature. In comparison to tactile methods, optical ones were considered notably faster but highly susceptible to the external environment, thus, appropriate isolation during the measurement is required [20]. It was emphasized by Pawlus et al. [21], that the type of surface topography can alter the discrepancies between the stylus and optical roughness measurements. De Lega et al. [22] studied the measurement reflectivity and smooth properties and found them to be crucial in the characterisation of the material's optical properties and layer thickness.

There are many types of errors affecting the accuracy of contactless surface topography measurement instruments among which, non-measured points (NMPs) are widely studied [23]. The impact of NMP presence on the ISO 25178 roughness parameter variations was analysed comprehensively and the range of errors was designated with consideration of different densities of light while measuring the surface [24]. Another type of optical error is extraneous effects in the point height of the measured workpiece known as individual peaks [25], outliers [26] or spikes [27]. The robustness of statistical methods for outlier identification was presented and improved by Wang et al. [28]. Spikes and batwings were removed by filtering technique based on the standard deviation presented by Le Goic et al. [29]. The standard deviation technique was also compared with morphological filters and slope methods by Podulka et al. [20] who found such an approach as an effective alternative for the spikes suppressions. On the other hand, Maculotti et al. [30] proposed a 'Gaussian process regression-based' approach for identifying and correcting outliers, providing a formal, robust, and univocally defined method to overcome surface topography measurement distortions.

Many studies were performed to avoid surface roughness metrology errors, defined as measurement noise. From the ISO requirements, the measurement noise is defined as the noise added to the obtained signal during the normal application of the measuring device [31]. Zuo et al. [32] measured the effect of noise on the estimated fractal dimension (EFD), relating it to the amplitude characteristics of the surface data. De Groot et al. [33] formulated the interpretation and proposed experimental methods for quantifying random areal contactless surface roughness measurement noise. For contactless coherence scanning interferometry (CSI), averaging the repeated roughness measurements or the fringe signal enlargement of the sampling frequency (often referred to as oversampling) could potentially reduce noise [34]. Vanrusselt et al. [35] compared plenty of optical surface topography measurement devices, including focus variations, confocal and coherence scanning instruments, for interpreting and specifying the measurement noise. However, there is still a large number of studies and guidance required when characterising the roughness measured by optical techniques [36].

One of the often-studied types of roughness measurement noise is high-frequency errors. Referring to its origin, can be acquired by the instability of the measuring mechanism and is simply caused by the outer vibrations [37]. The effect of the high-frequency noise on the ISO 25178 roughness parameters was found crucial for many types of machined topographies, including laser-melted, milled, honed, turned, ground, composite, ceramic and those with isotropic properties [38]. Sun et al. [39] reported, that the characteristic signals registered from the machined surface are a mixture of real signals and noise, proposing the wavelet denoising when features are characterised.

Frequency spectral analysis is often applied for the characterisation of various types of topographies, e.g. Jacobs et al. [40] determined many functional properties by using this method. Syam [41] proposed the general methodology for the implementation of fast and accurate measuring systems with optical in-process devices, particularly useful in industrial applications. Podulka [42] mixed the frequency-based techniques with the direction of the studied topographies indicating, that the definition of high-frequency noise is related to the process of selection of the data orientation, especially when considering both areal and profile characterisations. Dzierwa et al. [43] studied the influence of surface orientation on the surface measurement results with a comprehensive analysis of variations in ISO 25178 roughness parameters. The texture direction was found crucial in the characterisation of the influence of milled topography on the fatigue behaviour of magnesium alloy [44]. Macek et al. [45] proposed the correlation of areal, volume and fractal direction parameters for low-cycle fatigue tests, studying additively manufactured materials. Simultaneously, the fractal dimension was connected with a surface slope for steels after bending-torsion fatigue tests [46] and for the initiation stage of fatigue crack under bending-torsion studies [47].

Composite materials play a significant role in many surface quality improvement approaches by using various machining processes. Zhang et al. [48] reviewed the current advancements in the grinding treatment of composite materials and confirmed their importance in guaranteeing the final quality after the machining process. Adibi et al. [49] considered

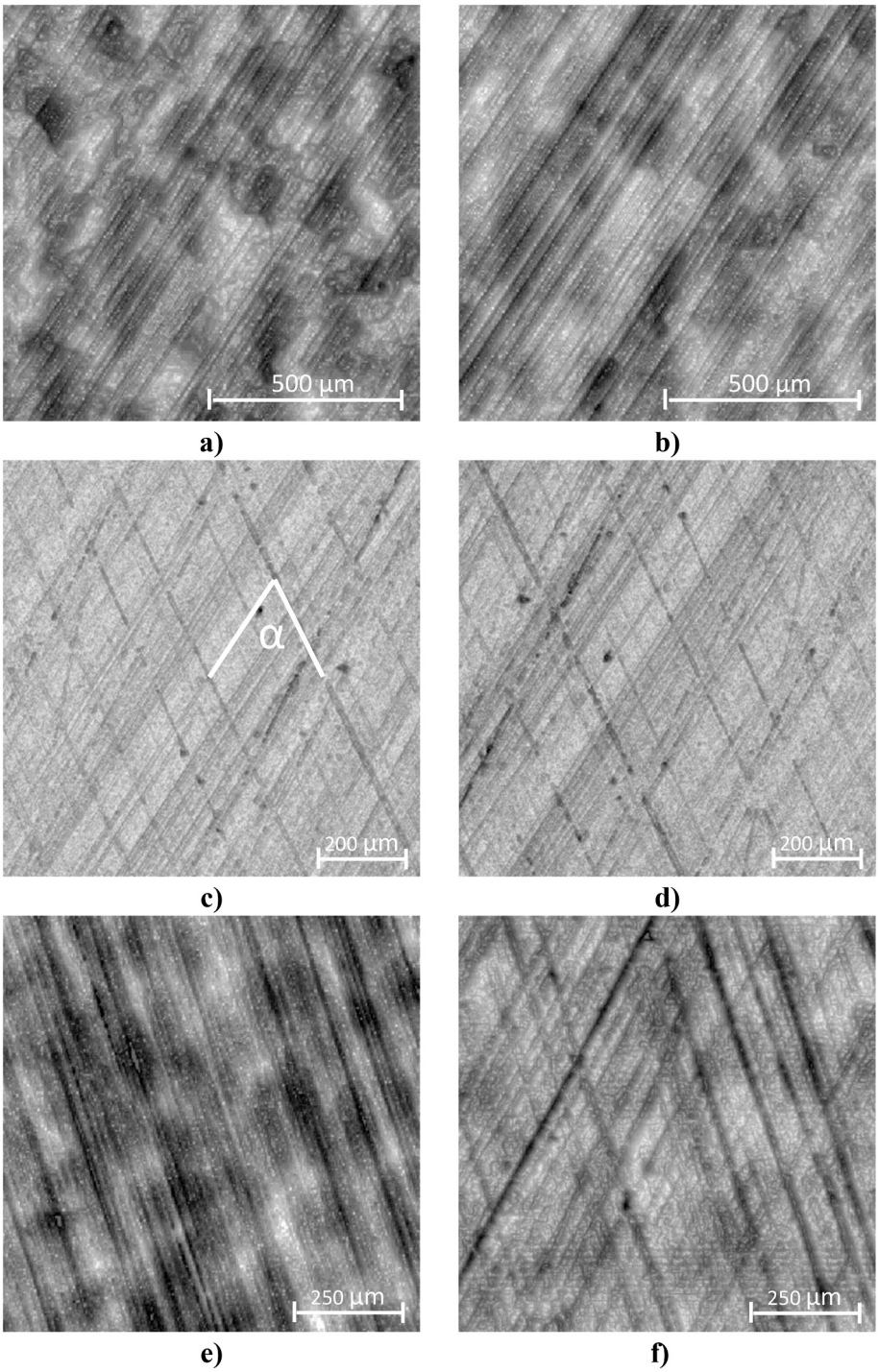

Fig. 2. Images of diamond-grounded ceramic (a,b) and honed composite (c,d) surfaces after initial (a,c) and final (b,d) stages of the machining process; milled ceramic surfaces after the final stage of machining in one (e) and two (f) directions; $\alpha = 60^{\circ}$.

the minimum quantity lubrication (MQL) in the grinding of ceramic matrix composites (CMCs) known for their low density, high values of hardness indicators, and outstanding thermal and chemical resistance. Balu et al. [50] supported the grinding modelling for titanium metal-matrix composites (MMCs) by connecting the indentation hardness, low- and high-stress belt abrasions, and the characteristics of surface grinding. Cao et al. [51] studied the effect of orientations of fiber in the ground woven ceramic matrix composites, providing a more detailed control in processing quality improvements. Generally, the fiber orientation influence on machinability during the grinding of ceramic matrix composite was studied and reviewed by Du et al. [52]. Zhu et al. [53] predicted surface roughness through the modelling of composite material behaviour during grinding. The authors measured its surface with a dedicated profiler and scanning electron microscope (SEM) instruments, combining the theoretical surface roughness model of aluminium alloy and silicon carbide. Azmir et al. [54] verified the influence of process parameters of abrasive water jet machining on epoxy composite surface roughness.

Machined ceramic surfaces were found by Samant et al. [55] as attractive for particular applications that in many cases are difficult to fabricate by traditional methods. An et al. [56] related those difficult-to-be-machined properties to the high brittleness, anisotropy, materials

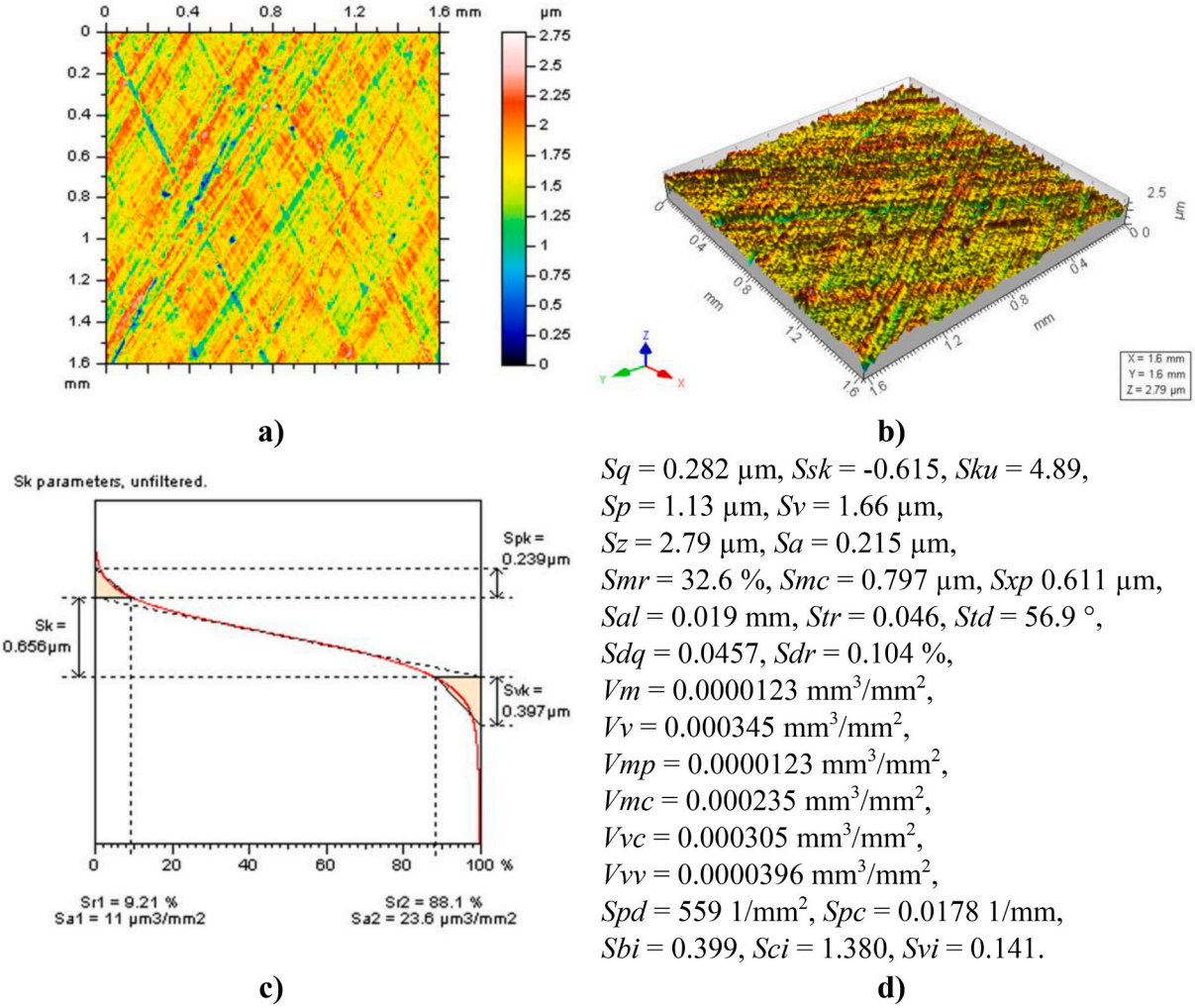

Fig. 3. Contour maps plots (a), isometric view (b), material ratio curve (c) and ISO 25178 parameters (d) of honed composite surface topography after wear tests.

heterogeneity, high mechanical and thermal loads and severe tool wear. Diaz et al. [57] reviewed the latest challenges in the machining of ceramic materials, including conventional and non-conventional methods. Pawlus et al. [58] reported prediction methods of surface textures subjected to the abrasive machining treatment. Singh et al. [59] employed a surface methodology analysis method for the central composite rotatable design experiment evaluating samples by SEM technique.

Except for difficulties in the machining of composite and ceramic materials, many issues could still appear when the raw surface topography data is processed. Excluding errors regularly found for optical methods, including NMPs, outliers, levelling and form removal processes, the reduction of errors caused by the environment plays a crucial role in an accurate description of surface properties. There are still many studies required in terms of measurement noise reduction. Thus in this paper, the type of measurement noise which is caused by the measuring system vibrations was studied during the characterisation of ceramic and composite machined surfaces. For the minimisation of the influence of high-frequency noise, the procedure with a direction consideration of surface machining traces is proposed. The variations in ISO 25178 roughness parameter values were studied according to the different noise-suppression filtering techniques verified with the proposed approach. The new methodology was proposed with an application of fast-implemented, available in the measuring instrument commercial software functions, using them in a proper order. Advancements were received due to a reduction in time compared to the common international method based on the measurement repeatability.

2. Materials and methods

2.1. Analysed surfaces and roughness parameters

In this paper, composite and ceramic materials were studied. Composite workpieces were subjected to the honing or milling processes. Considering the honing machining, the first step was boring, then, secondly, the slide-honed surfaces were received in a few stages process, including a diamond honing by vertical machine as rough, coarse and plateau honing steps. The cross-hatch value, the honing angle (α) was equal to 60°. The milling process parameters were used as follows: the rotational speed equal to 500 rev/min, the feed speed equal to 200 mm/min and the depth of cut equal to 10 µm.

The second type of specimens, ceramic workpieces, were processed with ground diamond or milling machining. The ceramic grinding process was performed at a rotational speed equal to 400 rev/min, a feed rate of 100 mm/min, and a total depth of dressing of 15 µm. The milling treatment parameters used in the study included the rotational speed of 400 rev/min, the feed speed of 100 mm/min and the depth of cut equal to 10 µm. The selection of the machining parameters was based on previous studies in the field of composite or ceramic surface treatments (Fig. 1).

Surfaces were studied in the initial and final stages of the machining processes. Furthermore, honed composite surfaces were analysed after

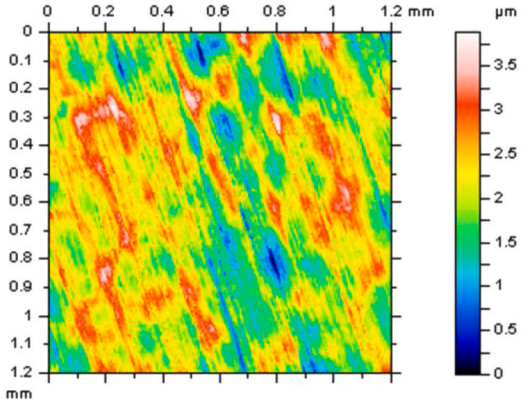

a)

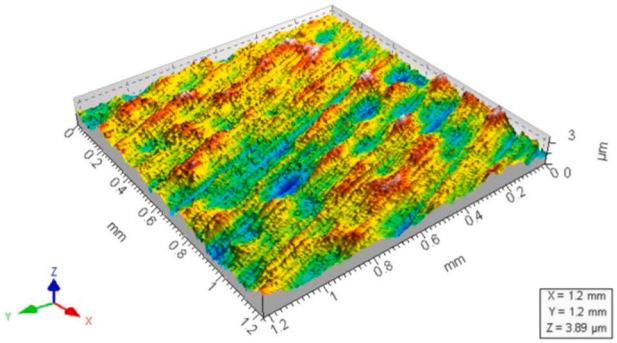

b)

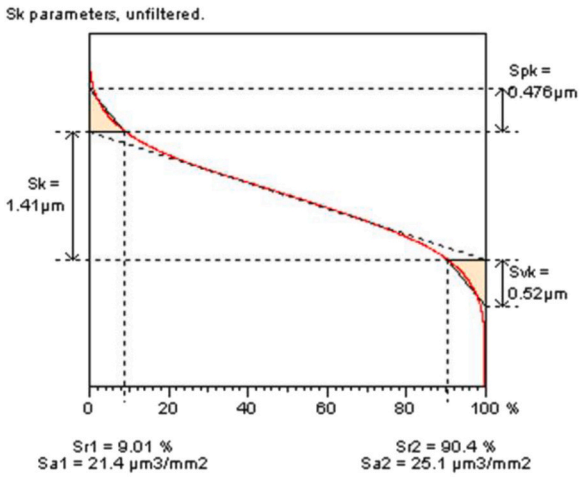

c)

Sq = 0.534 µm, *Ssk* = -0.0536, *Sku* = 2.94,
Sp = 1.8 µm, *Sv* = 2.09 µm,
Sz = 3.89 µm, *Sa* = 0.428 µm,
Smr = 6.77 %, *Smc* = 1.11 µm, *Sxp* = 1.07 µm,
Sal = 0.0613 mm, *Str* = 0.189, *Std* = 108 °,
Sdq = 0.0486, *Sdr* = 0.118 %,
Vm = 0.0000244 mm^3/mm^2,
Vv = 0.000708 mm^3/mm^2,
Vmp = 0.0000244 mm^3/mm^2,
Vmc = 0.000488 mm^3/mm^2,
Vvc = 0.000648 mm^3/mm^2,
Vvv = 0.0000602 mm^3/mm^2,
Spd = 210 $1/mm^2$, *Spc* = 0.0183 1/mm,
Sbi = 0.582, *Sci* = 1.55, *Svi* = 0.113.

d)

Fig. 4. Contour maps plots (a), isometric view (b), material ratio curve (c) and ISO 25178 roughness parameters (d) of milled ceramic surface topography after an initial stage of the machining process.

initial running-in abrasive wear tests. Wear tester under lubricated condition parameters included the normal load performed to 300 N, contact length ranging from 10 to 20 mm, and the total test duration equal to 35 min. Exemplary topography images of selected specimen surfaces are presented in Fig. 2.

Subsequently, the ISO 25178 roughness parameters were studied. It was confirmed, that surfaces subjected to the finishing milling can be described by the *Sq*, *Sal*, *Ssk* and *Sku* indicators and, as an alternative, the emptiness coefficient *Sp/Sz*, and parameters *Str*, *Spd* and *Sdq* could be studied as well [60]. One should highlight, that Sdq variation is responsive to the presence of high-frequency noise [61]. The peak curvature (*Spc*) and density (*Spd*) were also found as susceptible to high-frequency errors [62]. The characterisation of height parameters, additionally studying those from the Sk group, was also crucial as their values typically increased.

A study of variations of the ISO 25178 surface texture parameters according to the high-frequency measurement noise occurrence can be especially significant in that analysed errors can distort selected roughness parameters more than 100 % [36,62,71]. Alternative procedures for noise suppression, especially reducing the time of data processing by application of commonly used functions, can be valuable in that a large number of complicated and sophisticated methods can increase the number of errors due to the data evaluation.

2.2. Measurement procedure

The surface topography was acquired by using the contactless WLI instrument Talysurf CCI Lite including a standard sets: height resolution equal to 0.01 nm, 3.35 mm × 3.35 mm measured area with, correspondingly, 1024 × 1024 measured points and spacing derived as 3.27 µm. A Nikon, 5×/0.13 TI, lens was employed for all of the workpiece measurements. Around 20 surface topographies of each type of machined specimen were studied. In Figs. 3, 4 and 5, examples of studied surface topographies were presented.

For the computing of the ISO 25178 roughness parameters, the TalyMap Gold software by Digital Surf company was used. The same source was applied for the computation of functions used for the comprehensive analysis of the measured data, including power spectral density (PSD), autocorrelation function (ACF), and texture direction (TD). The PSD and ACF functions' mathematical formulas were precisely described in [64].

For the definition of the noise surface (NS), various filters were proposed: regular ISO 16610 Gaussian isotropic regression (GRF) [65] with robust modifications of Gaussian function (RGRF) [66], usual isotropic spline (SF) [67], closing and opening envelope morphological (MOF) [68] and fast Fourier transform (FFTF) [69]. The data rough thresholding technique was additionally investigated with an application of the software mentioned above. Advancements in the applications

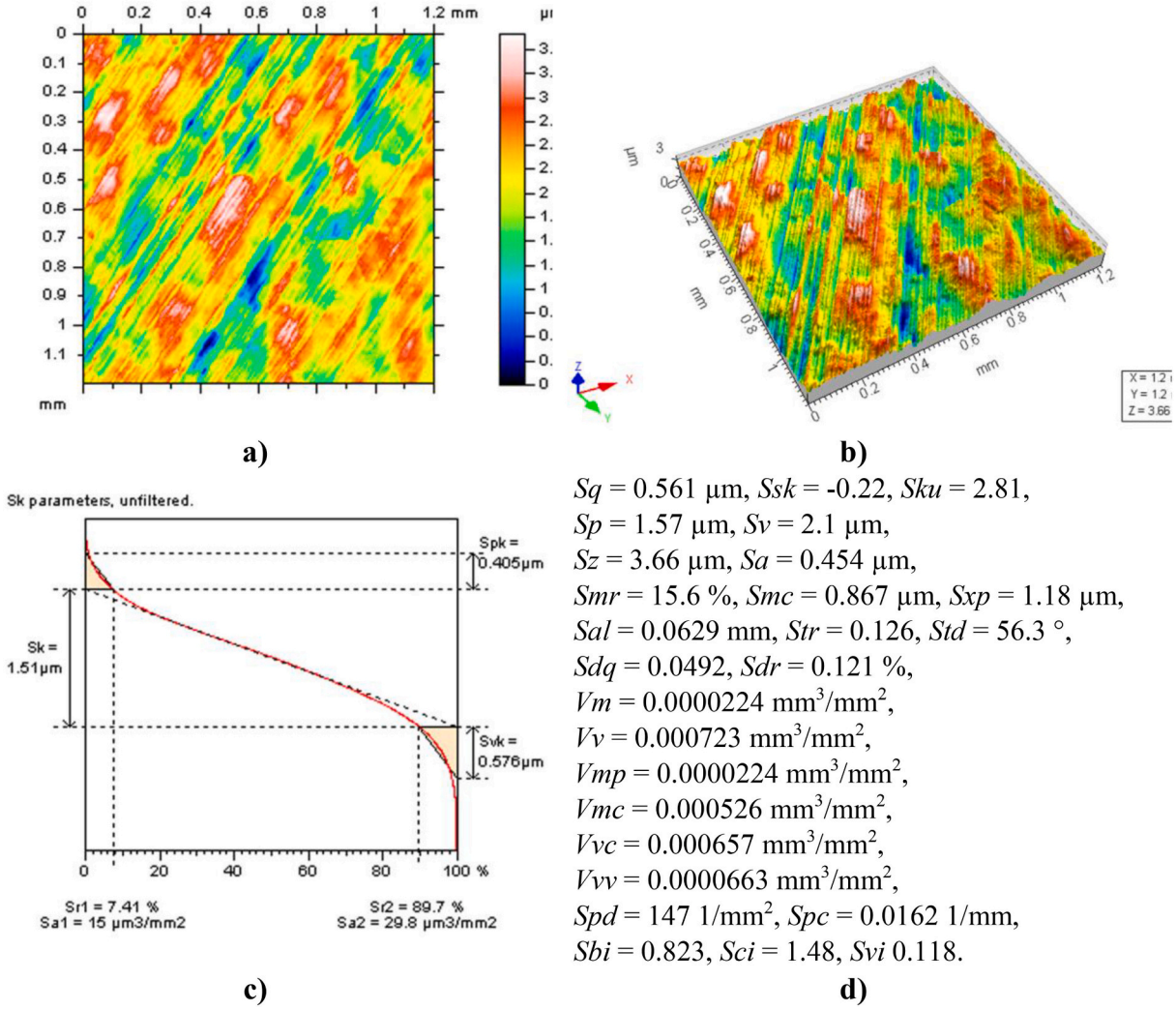

Fig. 5. Contour maps plots (a), isometric view (b), material ratio curve (c) and ISO 25178 parameters (d) designated from ground diamond ceramic surface topography.

of hard thresholding data according to the surface roughness characterisation have been already studied in previous investigations [70].

The main purpose of the paper is to mix the general functions and filters from the commercial software to improve the evaluation of the high-frequency measurement noise from the raw measured data of composite and ceramic surfaces after machining. Application of autocorrelation function, power spectral density method and texture direction plots, can be advantageous when applied simultaneously. Since computing all three functions is fast, proper application and its mutual improvements can be crucial for the suitable definition of high-frequency measurement data.

Usually, when applying a low-pass filter to express the high-frequency error data from the raw measured, the characteristic of the noise should be known before using filtration techniques [71]. Considering the international standards of measurement noise definition and reduction [31,72] repeating the measurement process at least three times with the same conditions and averaging the results seems to be the most reliable proposal. However, from the industrial performance, time-consuming methods are not allowed. The proposed methodology, improved on the comparison of the average results, can be an encouraging alternative to the measurement repeating process.

Since industrial performance requires reducing measurement time, which can simultaneously minimise the cost of the manufacturing process control systems, omitting the surface topography measurement process repetitions can be considered one of the daunting tasks to be performed. From the experimental proposals, the study of alternative procedures with fast implementations can be encouraging, especially with guidance from generally available functions. A fast executable approach with quick-calculated components may constitute an optimal solution for manufacturing process optimisations. Therefore, developing a procedure consisting of simple but well-organized operations may be more particularly prominent than complex and sophisticated methods, where a large number of influential factors can result in a greater susceptibility to data processing errors.

2.3. Data processing and roughness evaluation

For the definition of high-frequency errors from the measurement data, the noise surface (NS), was proposed. The noise surface is a surface retrieved after the application of a digital noise suppression filter [37]. Generally, when applying a digital filter in surface metrology, the data are divided into separate portions. Various decomposition approaches, based on the data digital filtration were proposed, examined and validated, considering the measurement of surface roughness [73]. One should highlight, that more sophisticated techniques are investigated as well [74], and many proposals involving the Gaussian function could be found in the literature [75]. Filters, depending on their properties, separate selected data from others. The general Gaussian filter,

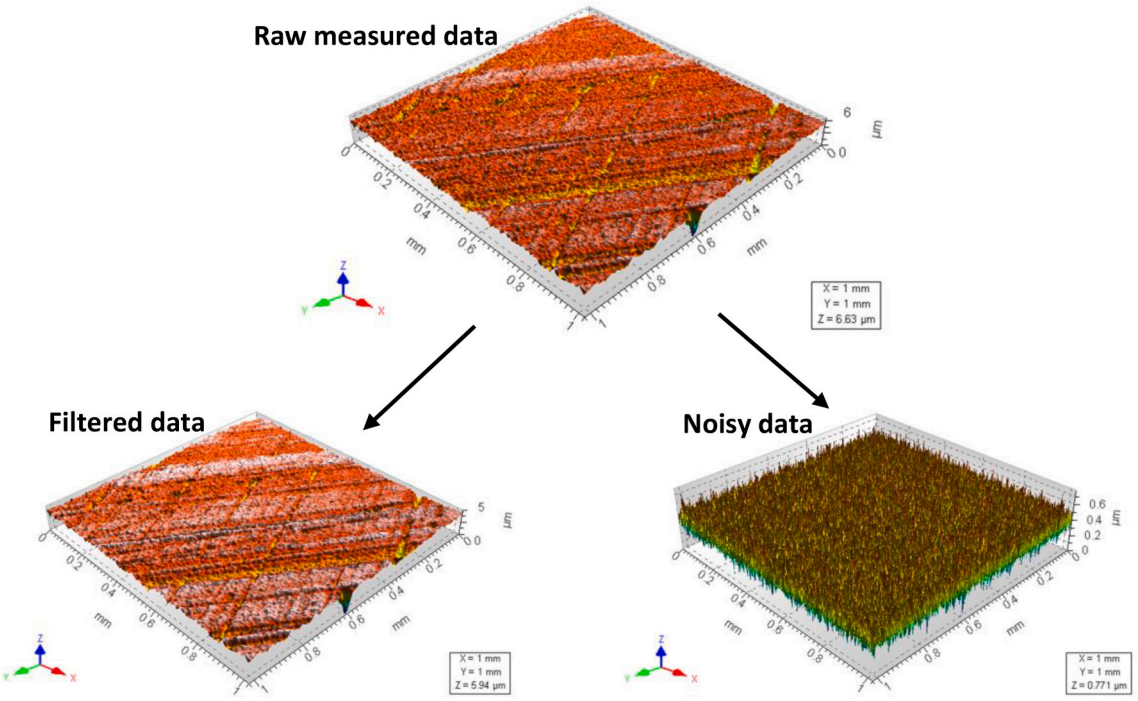

Fig. 6. Isometric view of the honed composite surface subjected to the decomposition by application of spline filter, cut-off = 5 μm.

considering the surface topography data, separates it into a long- and short-frequency portion of information. In the proposed technique, the high-frequency data are designated as the 'noise surface'.

In previous studies by Podulka [76], it was confirmed, that properly obtained (filtered) NS should include several basic properties:

(1) it must consist of high-frequency data or such data should be dominant (PSD studies);

(2) it should be isotropic, even if the machined surface is not (TD analysis);

(3) their ACF must have proper shape [77].

The main aim of the proposed procedure was to improve the verification of the (2) issue. Surfaces after ground, honed and milled treatments, are topographies with deterministic patterns, where examples of this type of textures were comprehensively studied by Jiang et al. [78]. For the specimens considered, one or two dominant directions were obliged. Studies of NS isotropic characteristics can be further improved with eye-view analysis or extraction of profiles, and application of hard data thresholding method. Fig. 6 shows an example of noise spline filtering decomposition of the raw data measured by the WLI instrument from the honed composite surface, in which the noisy data is the noise surface.

In this research, it was newly proposed to analyse the NS profile data with an examination of profile heights. In practice, the environment vibration affects the measured probes equally [79]. In addition to those issues, it was proposed to study whether the NS contains a homogenous quality in all of the retrieved data. Furthermore, the heights of the profiles extracted from one NS, e.g. obtained by Gaussian filtering, should be similar or, at least, should not be significantly different.

It was found in previous comprehensive studies that the direction of profile data extraction can significantly influence the process of characterisation of the received data [76,77]. Therefore, secondly, the direction of profile extraction from the NS data can be oriented towards the machining direction. Such an approach can be also improved if the treatment-trace profile heights are similar to those where the machining was not detected or its influence was negligible. In light of such findings, the NS can be highly advantageous for the selection of digital filtering methods and their cut-off value.

Both these properties are indicated in Fig. 7. The profiles extracted from the NS should be, firstly, located in the same area where the machining traces are on the measured surface and, secondly, their direction must be the same as the direction of the machining process.

When comparing the properties of the NS, an appropriate cross-hatch angle must be maintained. In Fig. 8, the procedure of profile orientation and location selection was presented for the milled composite surface after two directions of the machining process applied. Profiles were designated horizontally (P3) and according to the valleys formed during the machining process (P4 and P5).

In further comparative studies, where noisy data received by FFTF and RGRF methods are correlated, the differences in the maximum height of the profiles, Pt, provided some confidentiality. In Fig. 9, the Pt values of profiles P3, P4 and P5 were contrasted for both filtering techniques. In the case of the FFTF approach, the variations were usually lower than 15 %. On the other hand, for the RGRF application, they were higher than 30 %. Simultaneously, the maximum height (*Sz*) of the NS was 1.4 μm and 3.28 μm for the FFTF and RGRF scheme, respectively. Considerable differences were observed with the differences in the noise amplitude.

For the suppression of the high-frequency components from the measured data, different filtering techniques were proposed. One should mention, that commonly used and often verified are Gaussian function-based filters. In the proposed study, the regular Gaussian isotropic regression filter (GRF) and, secondly, its robust modifications (RGRF) were applied accordingly. The robust modification of the Gaussian function processing was considered significant in many metrological problems, including the reduction of the end-effect of the data filtering [80].

Some advances were proposed with a spline filter (SF), which was obliged to be less dependent on the sampling interval during the measurement process [81]. Lou et al. [82] defined the morphological filter (MOF) as more suitable for the prediction of the functional performance of machined components than general mean-line-based filters. Podulka et al. [83] indicated the benefits of envelope characteristics for surface texture analysis. Zakharov et al. [84] emphasized the asymmetric benefits of morphological filtering techniques for roughness evaluation.

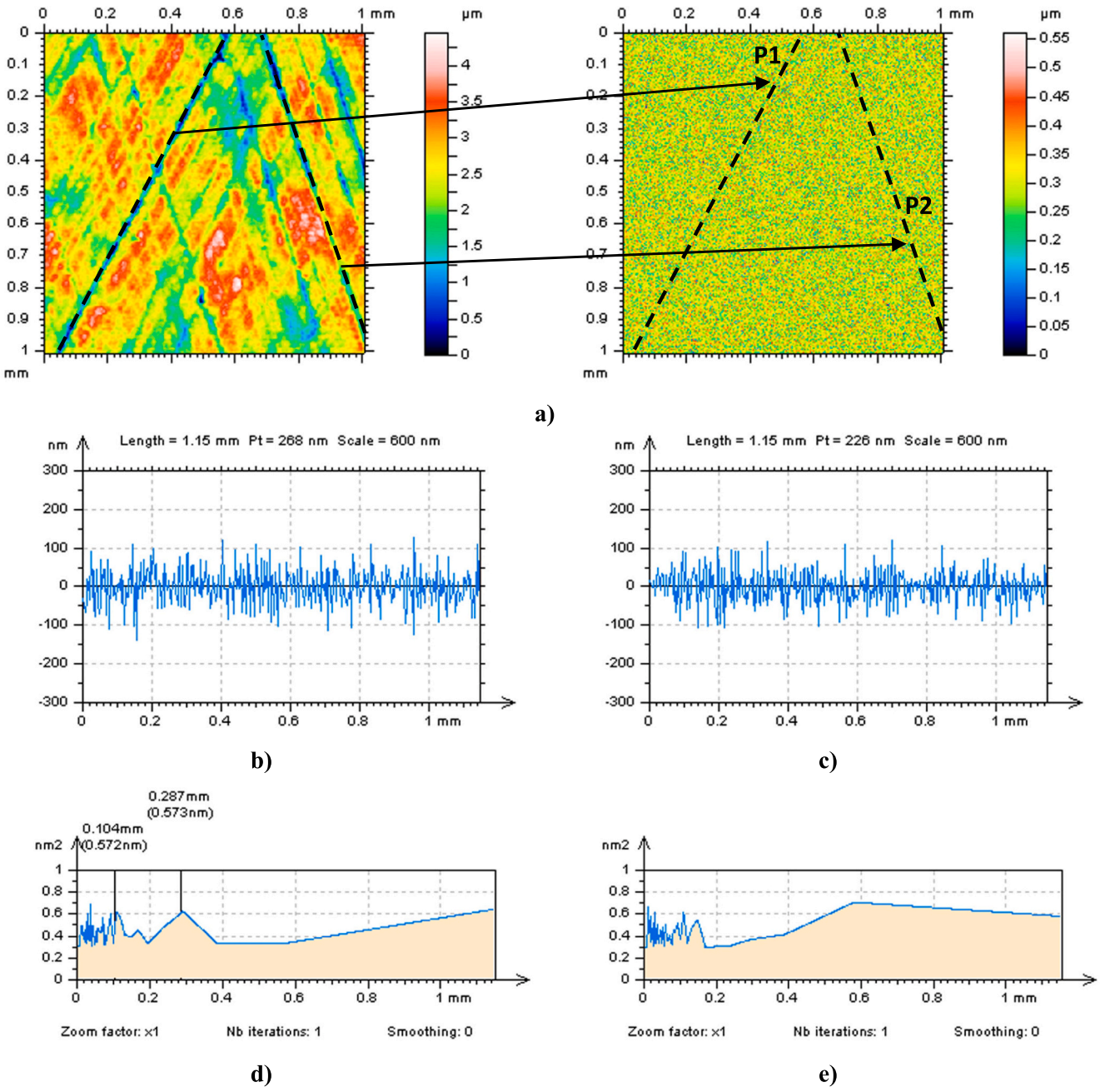

Fig. 7. Contour map plots of the milled ceramic surface and the NS received by the usage of SF with cut-off = 5 μm (a) and profiles P1 (b) and P2 (c) with their PSDs (d,e), respectively.

Furthermore, the fast Fourier transform (FFT) was introduced by Tien et al. [85] as effective for the analysis of the results from optical thin film surface roughness measurement. All of the filtering methods were compared with proposed procedure improvements.

2.4. *Proposed procedure for roughness characterisation*

Fig. 10 presents the flow chart of the proposed procedure. Firstly, the raw WLI measured data were filled in with non-measured points (NMPs) by a method based on the mean value of the neighbour points. Secondly, data were levelled using a least-square plane (LSPL) method, available in the commercial software. Finally, outliers were removed by the usage of the hard data thresholding technique. The thresholding ratio value was established as 0.13 % – 99.87 %, as evaluated in the previous machined surface roughness analyses [70,76].

After LSPL and outlier pre-processing, the procedure of reduction of the high-frequency measurement noise is applied. The selection of the proper filter and its cut-off is validated with profile characterisation. It was found, that areal and profile studies could be designated as equally important in many metrological issues [86]. The profile characterisation was found especially crucial in the improvements of the detection and removal of high-frequency errors from the results of honed surface topography measurements [87].

According to the isotropic properties of the noisy data, indicated as NS, extraction of profiles in various directions could be compared. Lacks in the TD characteristics of the NS data could be justified by the height and density of the received data, using a PSD, ACF and analysis of the height *Pt* of the profiles.

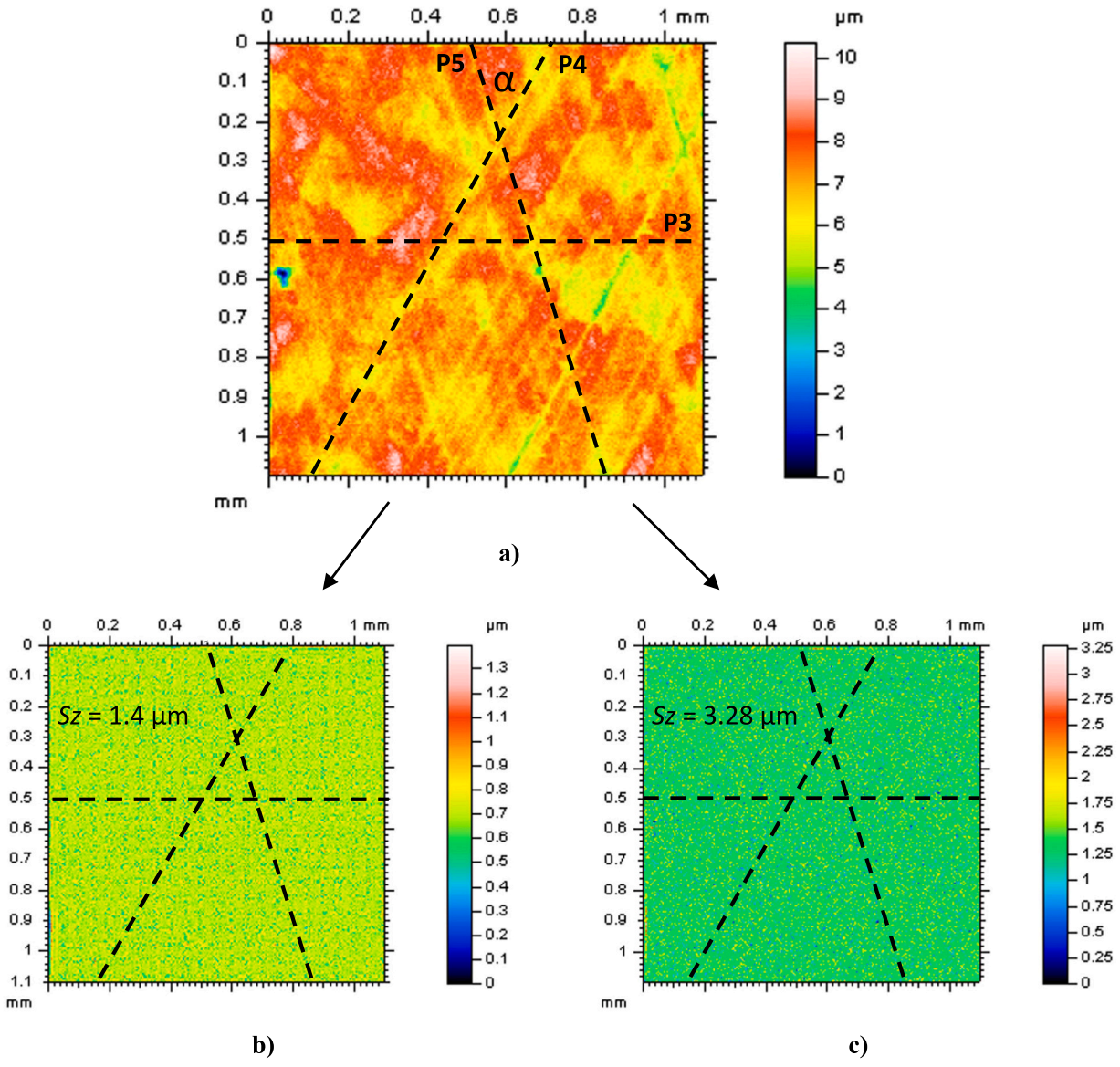

Fig. 8. Contour map plots of the measured milled composite surface (a) and the noisy data received by the usage of FFTF (b) and RGRF (c), cut-off = 7.5 µm.

In Fig. 11, the development of the profile validation method was presented. The raw measured data were subjected to digital filtration after pre-processing with LSPL and outlier removal processes. The selection of a suitable filter with a cut-off value was verified with a few-step analysis.

Firstly, the noisy data, NS, were studied visually. According to the required properties designated for the high-frequency noise surface, the NS must contain only components located in the high-frequency domain or this domain should be dominant. In practice, the NS should not consist of any non-noise features, including e.g. treatment traces. If the non-noise data were not detected visually, the hard thresholding technique was employed additionally.

Secondly, the frequency-based studies of NS were performed with PSD and ACF characterisations. The power spectral analysis, PSD, enables to restrict the calculations if data contain the high-frequency components as those dominant. One should emphasise, that analysis of the shape of autocorrelation operation, ACF, could potentially affect the detection of high-frequency data more considerably.

Finally, the total height of the profiles, Pt, extracted from the noisy data in various directions, was compared with receiving the final response. Including the isotropic properties of NS and similar total heights of the variously oriented profiles, the multithreaded characterisation of the high-frequency noise-suppression method was improved.

3. Results and discussions

3.1. Advantages of profile characterisation over areal assessments in the evaluation of high-frequency noise

Measurement and study of surface roughness are subjected to an areal performance that, considering their nature, most surface interactions are areal. It was found, that 3D texture parameters are more reliable than those from the 2D characterisation [88]. However, the study of selected types of surface topography measurement errors was improved with a 2D characterisation, as PSD and ACF studies gave more direct responses, especially when surface data contained machining features [89]. Valleys and scratches created by the honing, grinding, milling and burnishing techniques, can vary the accuracy in the definition of high-frequency errors with PSD function applications. The width, height and density of the feature were designated as significant

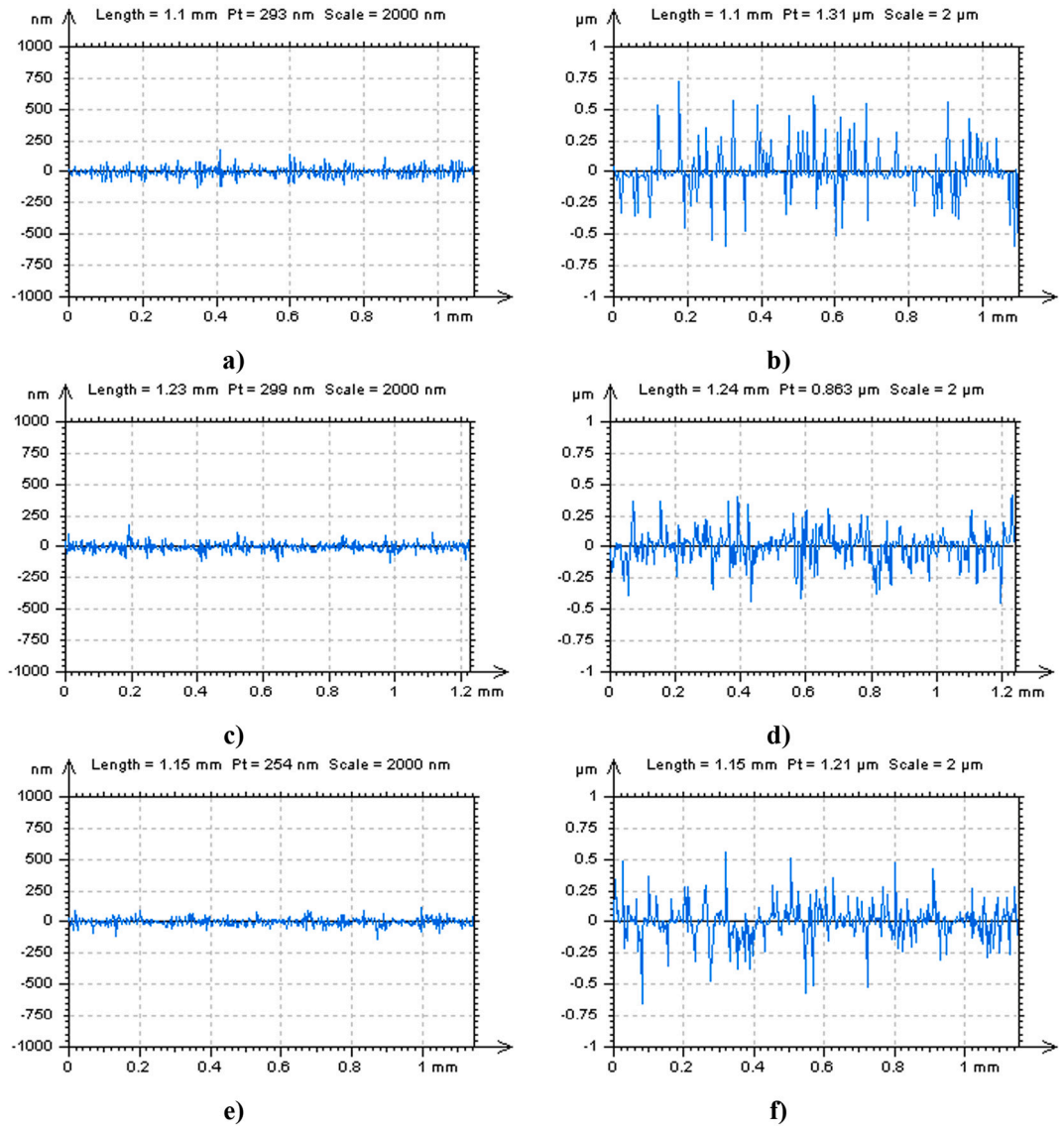

Fig. 9. Profiles extracted from NSs obtained by 7.5 μm FFTF (a,c,e) and RGRF (b,d,f) filtering techniques, received in the location: P3 (a,b), P4 (c,d) and P5 (e,f), description in Fig. 8.

for high-frequency measurement noise studies when compared to many advanced spline filtering techniques [90].

In Fig. 12, the PSD definition of the frequency composition of surface topography was presented. It was found, that an areal PSD study of the high-frequency components was difficult to observe for machined composite or ceramic surfaces, like honed, ground or milled specimens. According to previous studies, the high depth of the features, including dimples, valleys or scratches, caused a decrease in the precision of the PSD noise detection. Therefore, an additional profile characterisation with orientation compliant with the direction of the machining process was employed. Fig. 13 contains an example of extracted profiles from honed composite and milled ceramic surfaces in a direction according to the treatment traces. From the analysis of PSDs, it was assumed, that the high-frequency data are included in the results of WLI measurements, as marked by the arrows.

In Fig. 14, NSs filtered by various techniques were studied and compared. When considering a properly defined NS, it should not contain any non-high-frequency-noise features, like scratches or valleys. From the visual characterisation of NS, the non-noise features for the data filtered by MOF and FFTF techniques were identified, as indicated by the arrows. As could be observed, the directions of non-noise features and machining were matched. Initially, those filtering approaches were not appropriate for the removal of high-frequency noise.

The non-noise components detection improvement was proposed with thresholding data. The thresholded RGRF NS was designated with machining traces, as demonstrated by arrows. From the optical analysis of the NS contour map plots, the most encouraging results were assigned to SF applications. The isotropic properties can be justified with this method, where the NS data (Fig. 13c) and thresholded NS data do not contain non-noise patterns. In practice, the fewer feature direction traces are detected the more isotropic NS properties can be designated.

Multithreaded confidentiality can be proposed with a study of the PSD and TD functions. Since spectrum analysis can retain information on the frequency composition of the data, the texture direction could be beneficial in the isotropy examinations. In Fig. 15, both PSDs (left column) and TDs (right column) explorations are displayed. Whereas frequency studies stated SF and FFTF advantages over RGRF and MOF techniques (marked by the arrows), the isotropic characteristic was concerned only with the SF method.

TD graphs showed that RGRF, MOF and FFTF contained the first dominant direction related to the orientation of the machining processes. Contrarily, the first direction of the NS filtered with SF was not

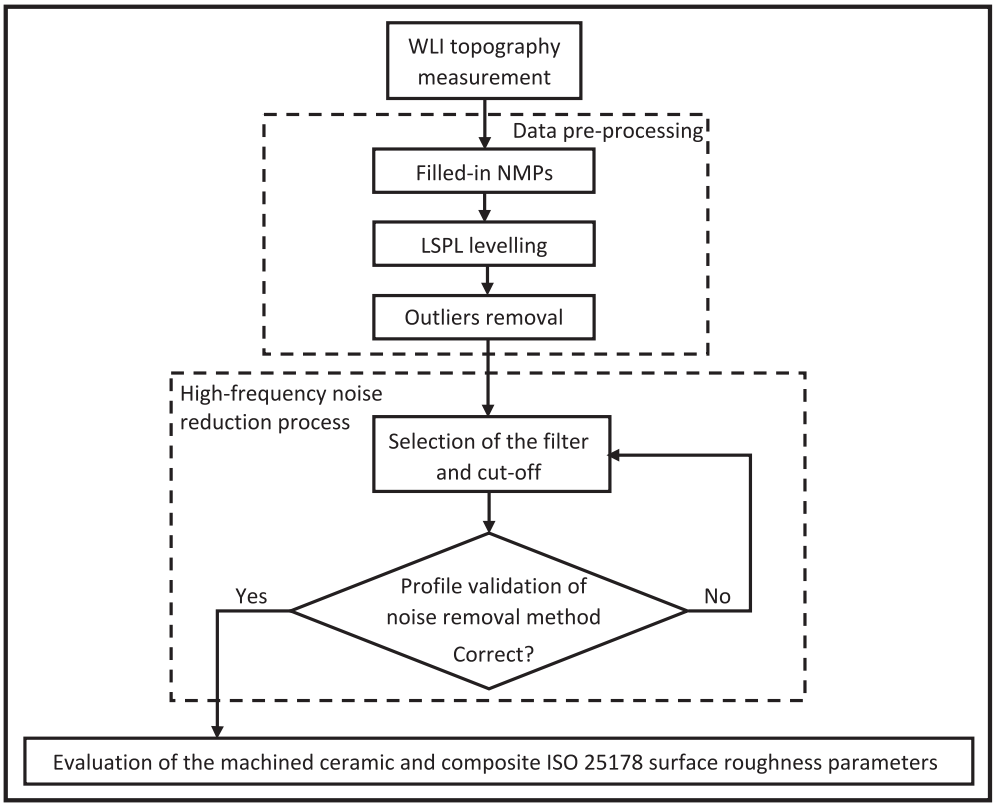

Fig. 10. The flow chart designated for the applied procedure.

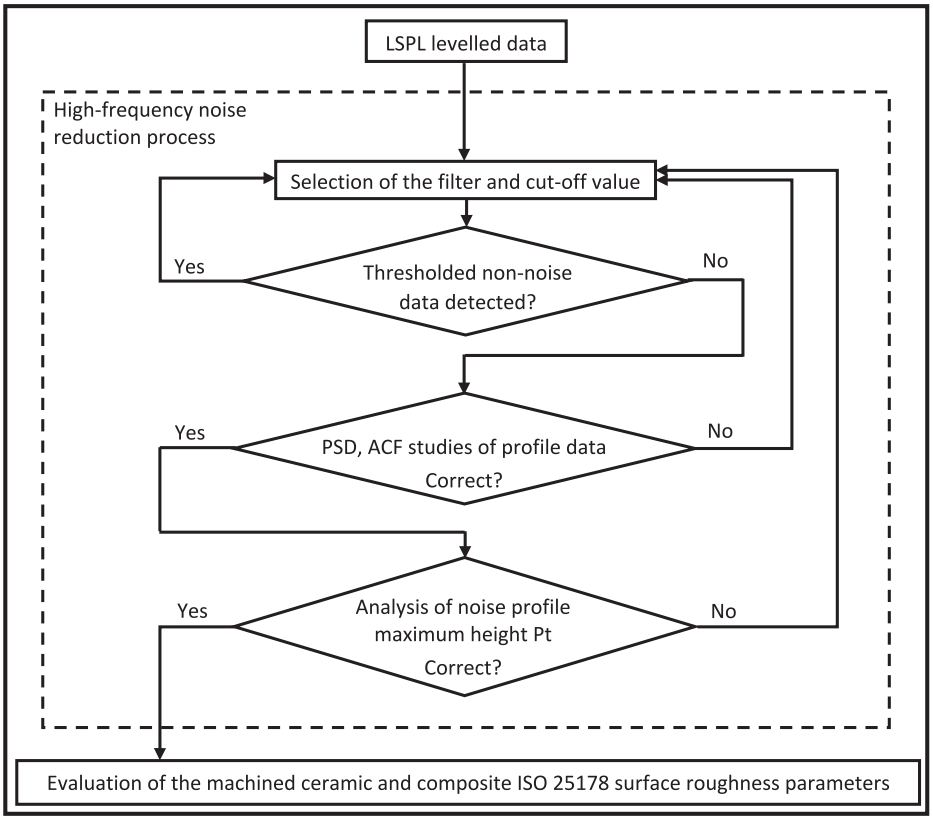

Fig. 11. The flow chart of the profile validation method.

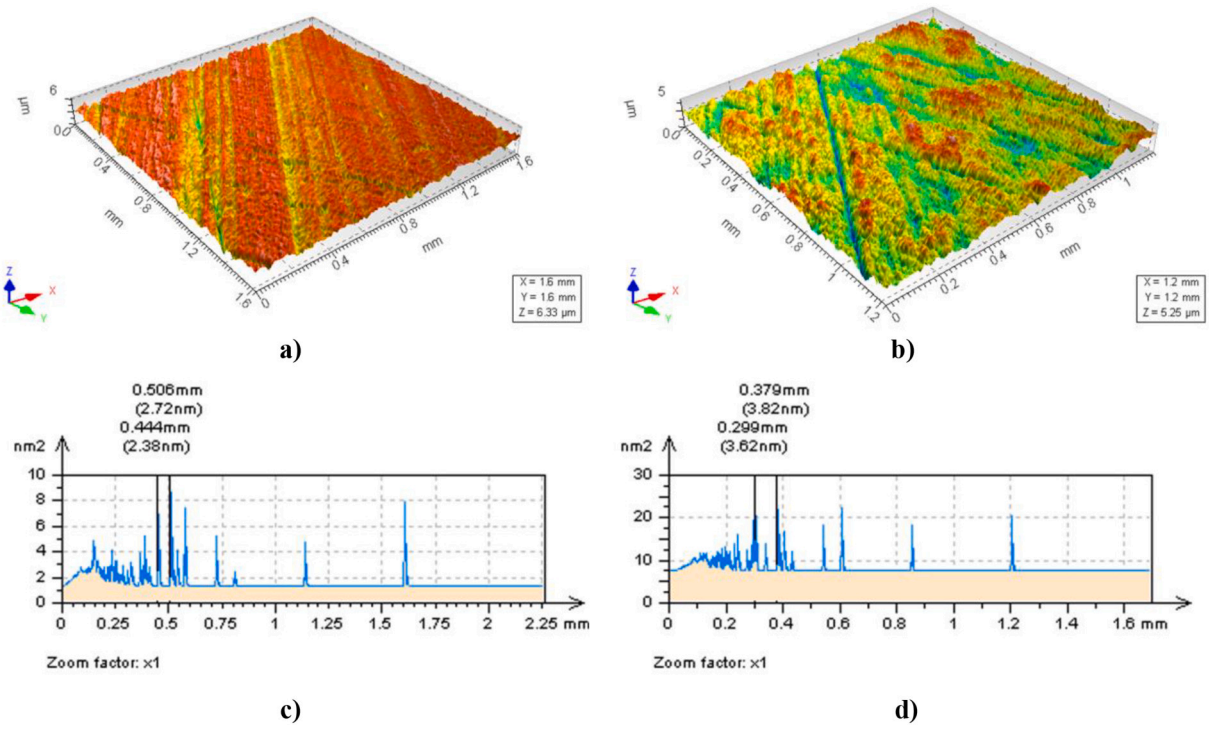

Fig. 12. Isometric view of honed composite (a) and milled ceramic (b) WLI measured surfaces and their PSDs (c,d), respectively.

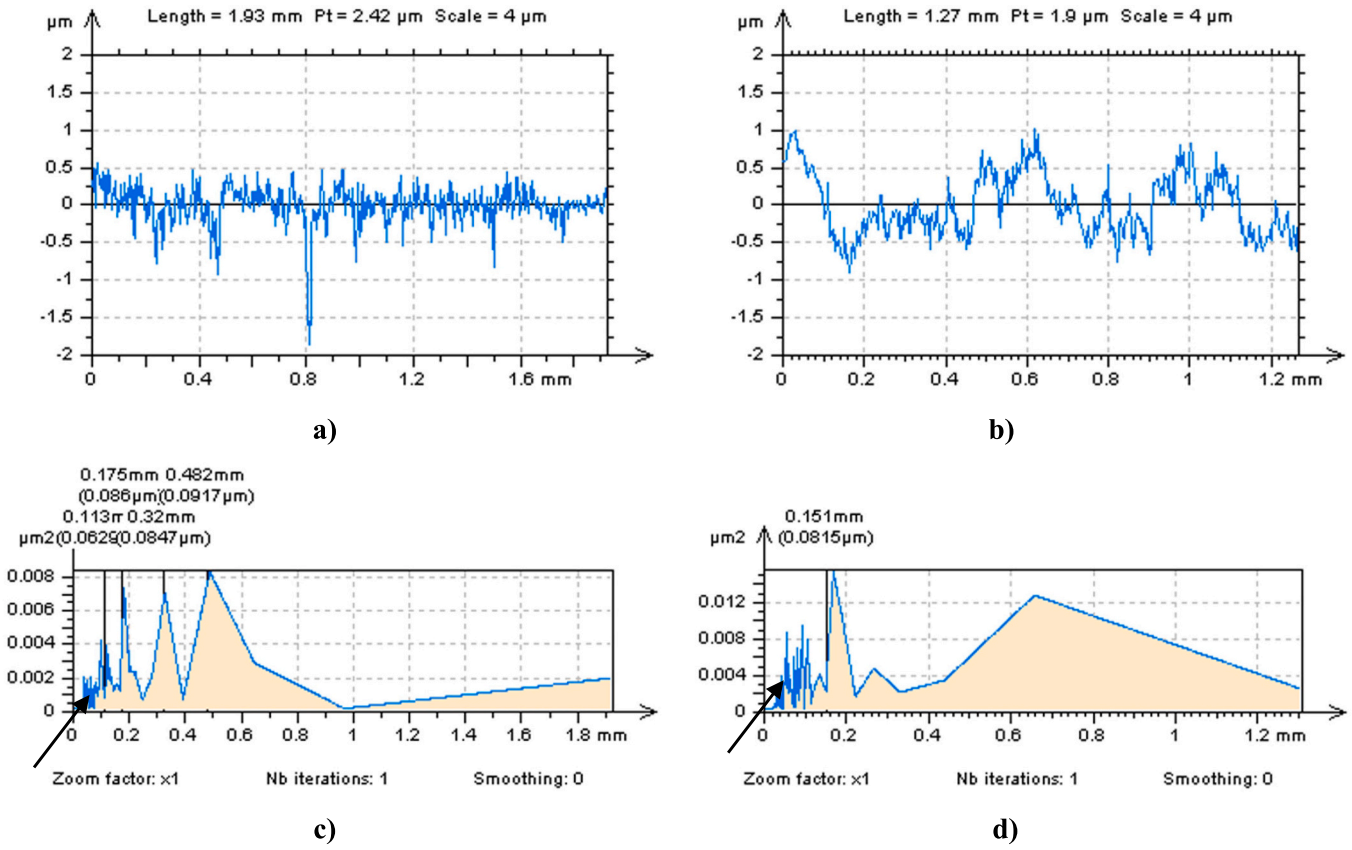

Fig. 13. Profiles extracted from the honed composite (a) and milled ceramic (b) WLI measured surfaces with treatment trace direction, and their PSDs (c,d), correspondingly.

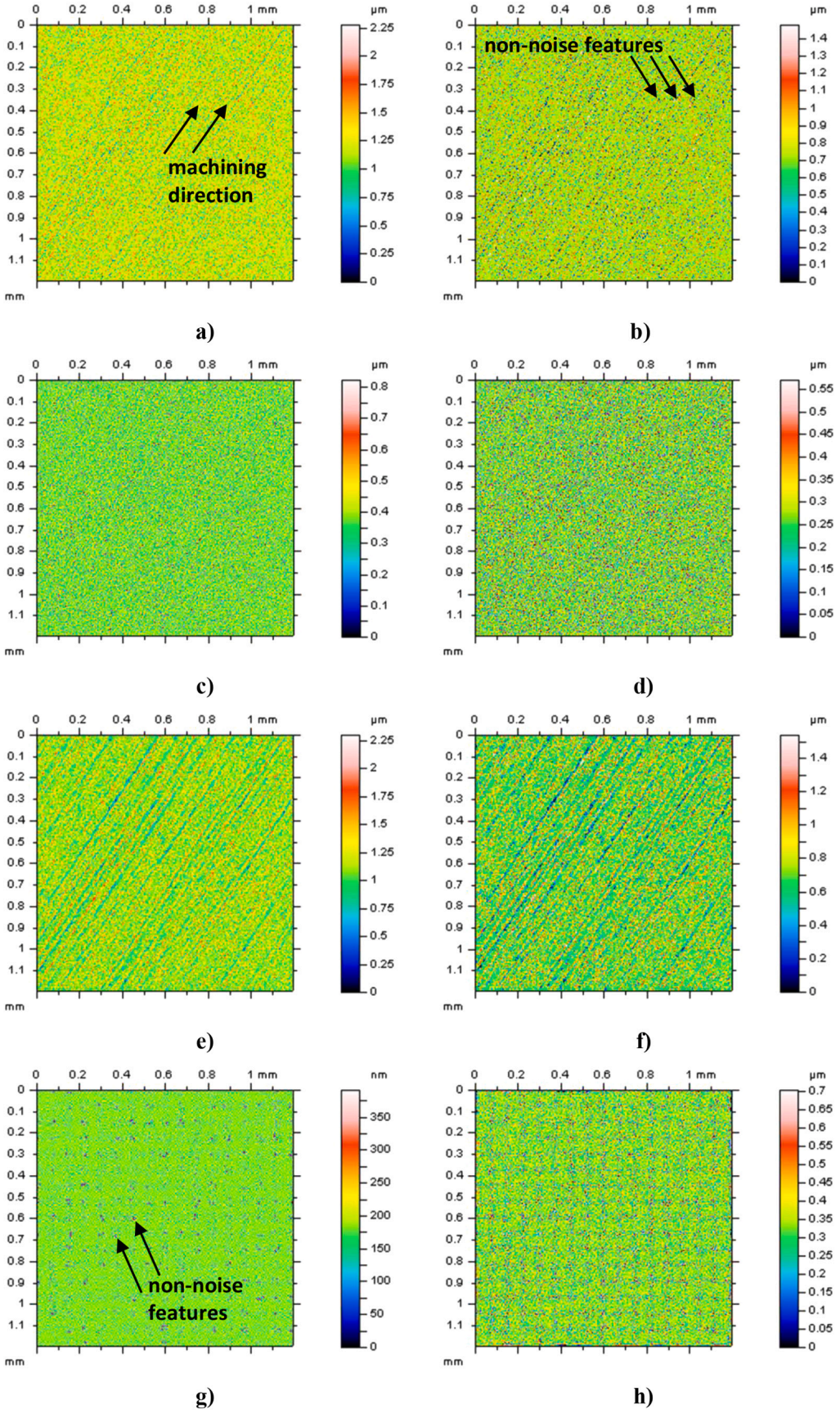

Fig. 14. Contour map plots of NSs obtained by application of RGRF (a), SF (c), MOF (e) and FFTF (g), cut-off = 7.5 μm, received from the ground ceramic surface, and their thresholded (0.13 %–99.87 %) NSs (b,d,f,h), respectively.

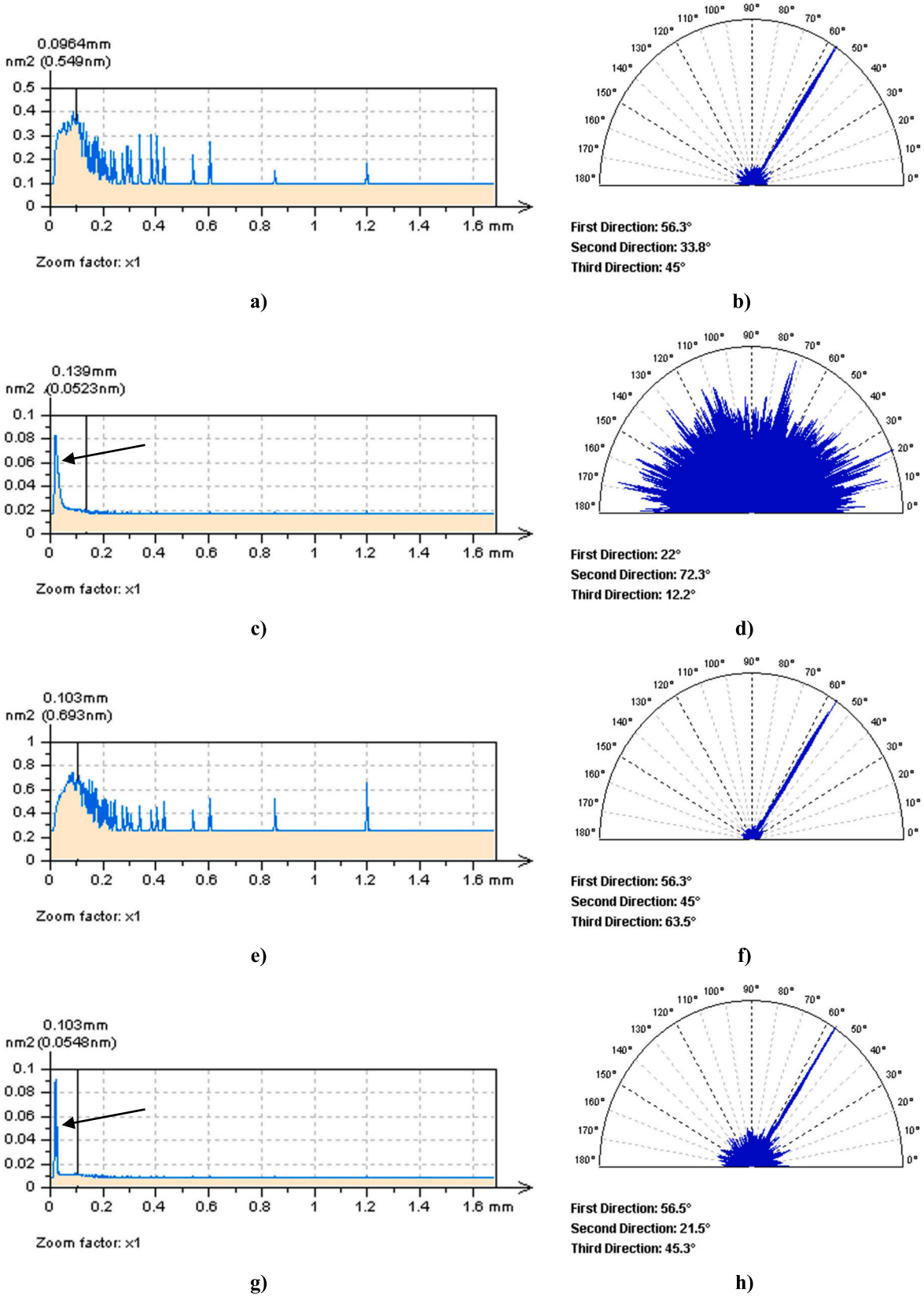

Fig. 15. The PSDs (a,c,e,g) and TDs (b,d,f,h) of thresholded (0.13 %–99.87 %) NSs obtained by application of RGRF (a,b), SF (c,d), MOF (e,f) and FFTF (g,h), cut-off = 7.5 μm, received from the WLI measurements of ground ceramic surfaces.

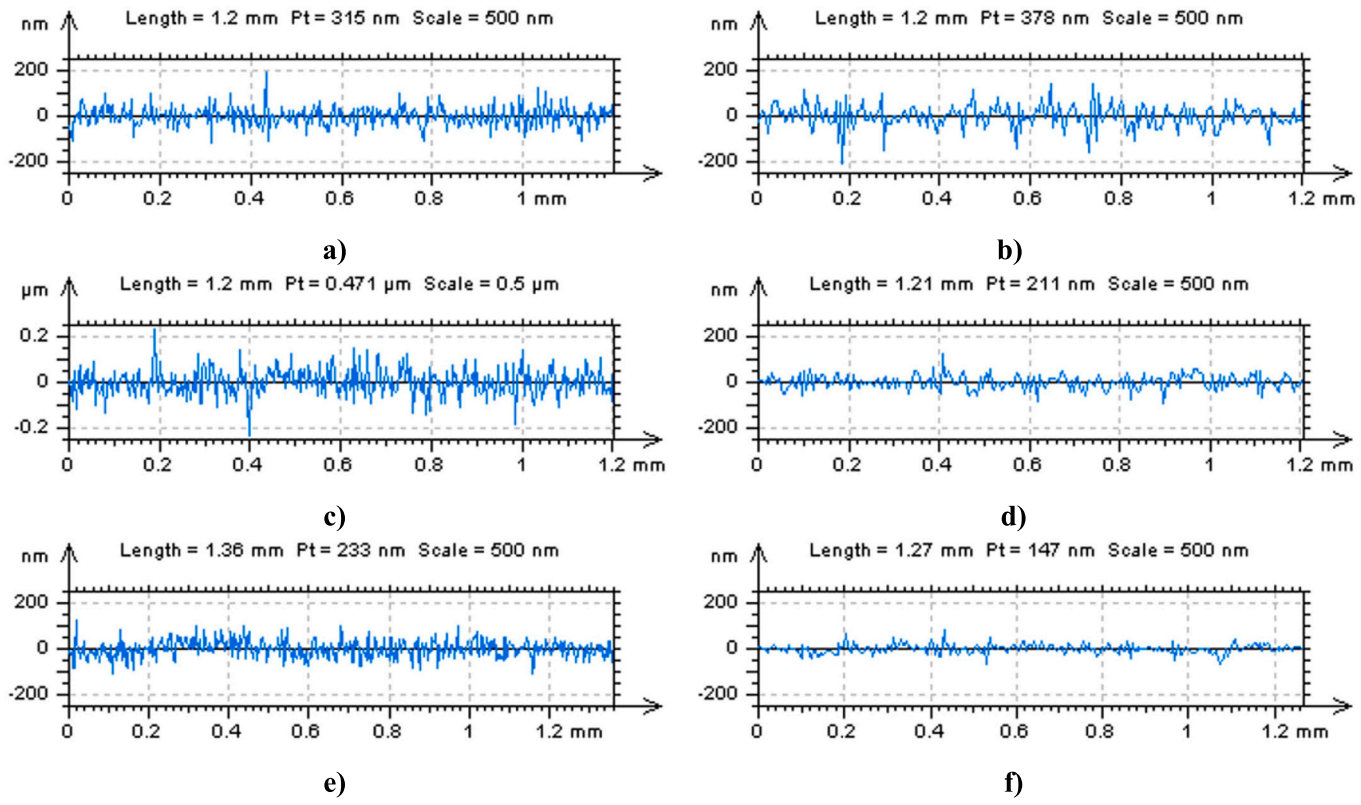

Fig. 16. The profiles extracted from the NSs obtained from WLI measured milled composite (a,c,e) or ceramic (b,d,f) surfaces by application of GRF, cut-off = 7.5 μm, in the horizontal (a,b), vertical (c,d) and machining (e,f) directions.

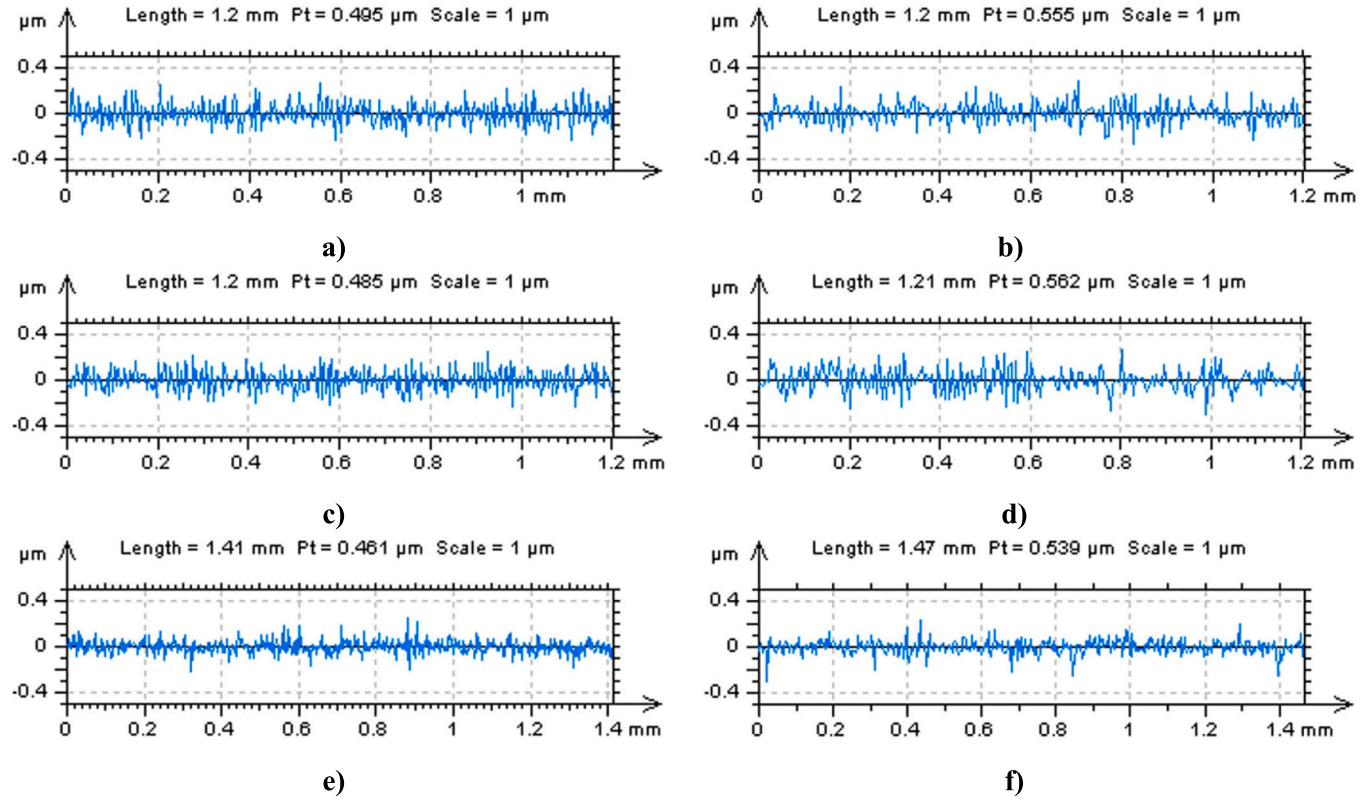

Fig. 17. The profiles extracted from the NSs obtained from WLI measured milled composite (a,c,e) or ceramic (b,d,f) surfaces by application of SF, cut-off = 7.5 μm, in the horizontal (a,b), vertical (c,d) and machining (e,f) directions.

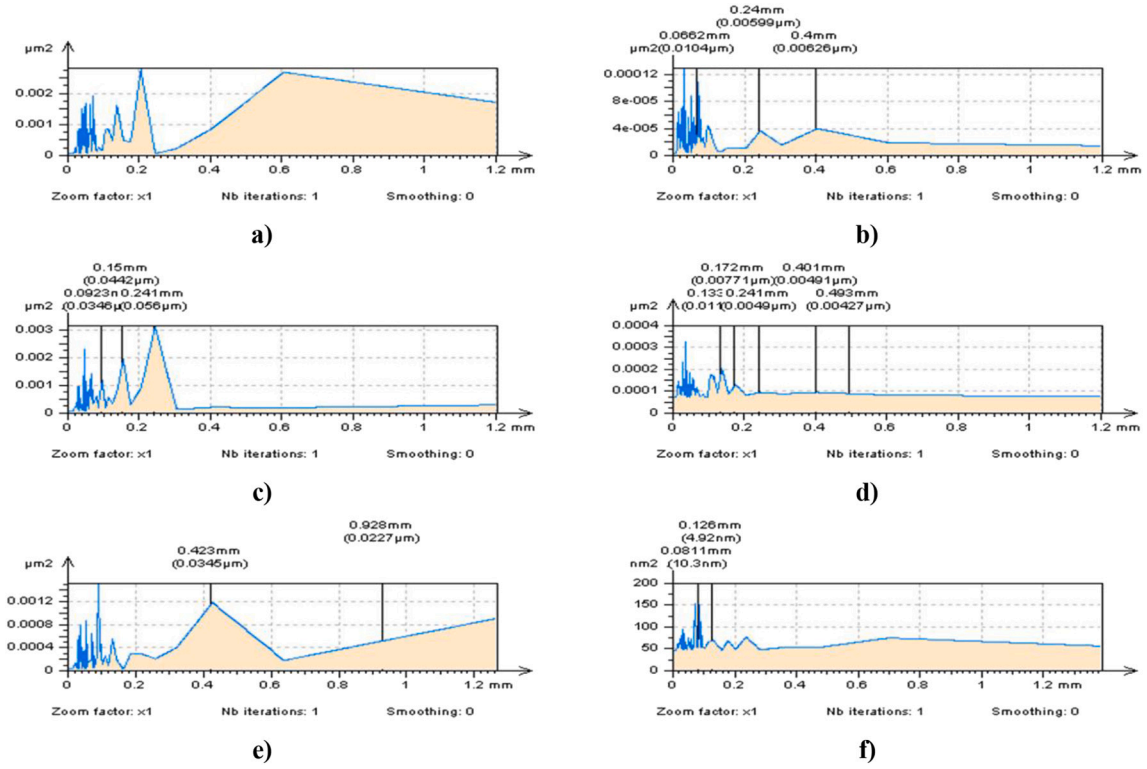

Fig. 18. The PSDs of profiles extracted from the NSs obtained from WLI measured milled composite surfaces by application of GRF (a,c,e) or SF (b,d,f), cut-off = 7.5 μm, in the horizontal (a,b), vertical (c,d) and machining (e,f) directions.

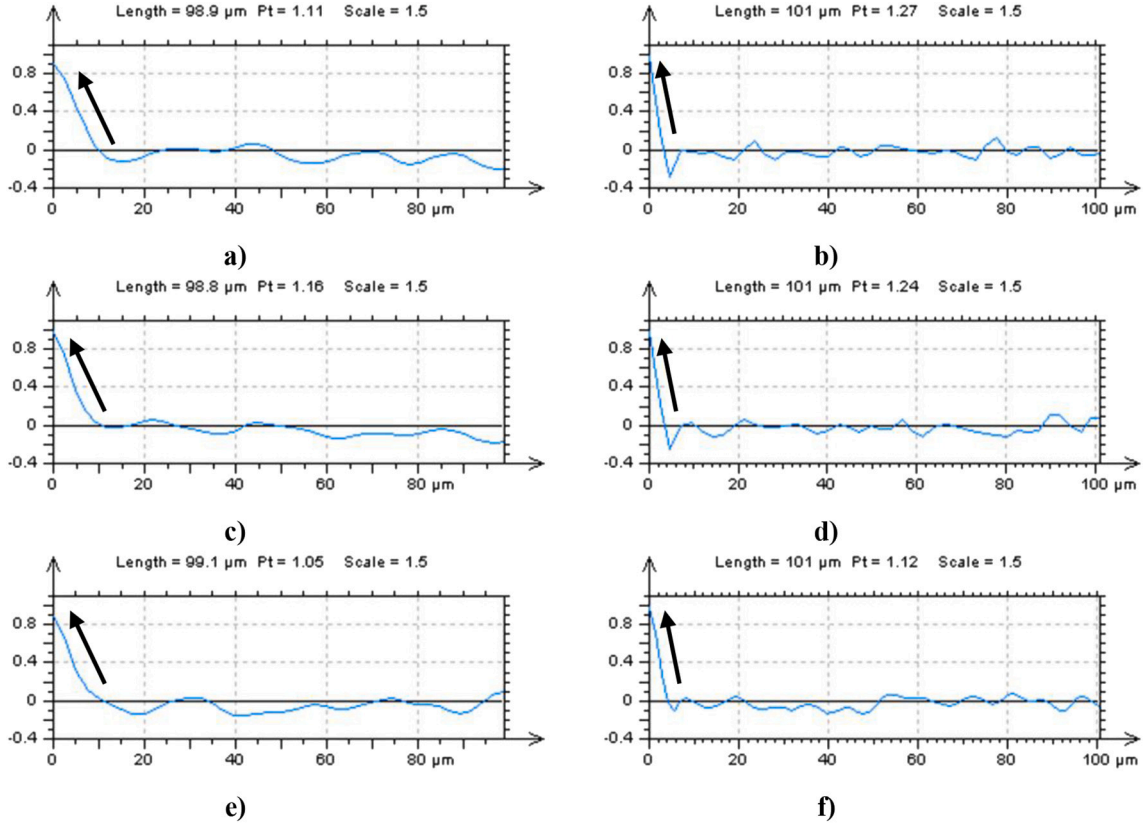

Fig. 19. The ACFs of profiles extracted from the NSs obtained from WLI measured milled composite surfaces by application of GRF (a,c,e) or SF (b,d,f), cut-off = 7.5 μm, in the horizontal (a,b), vertical (c,d) and machining (e,f) directions.

Table 1
The ISO 25178 roughness parameters of machined ceramic surfaces, calculated for the measured data and those after noise filtering by various techniques.

Groups and parameters		Units	Ground diamond ceramic				Milled ceramic			
			Raw measured	RGRF	SF	FFTF	Raw measured	RGRF	SF	FFTF
Height parameters	*Sq*	µm	0.593	0.554	0.568	0.565	0.637	0.599	0.617	0.611
	Ssk		−0.194	−0.187	−0.208	−0.203	−0.327	−0.321	−0.352	−0.349
	Sku		2.85	2.8	2.82	2.82	3.23	3.16	3.24	3.23
	Sp	µm	2.03	1.67	1.77	1.7	2.44	1.97	2.16	2.07
	Sv	µm	2.34	2.16	2.14	2.19	2.81	2.61	2.67	2.66
	Sz	µm	4.37	3.83	3.91	3.88	5.25	4.58	4.83	4.74
	Sa	µm	0.478	0.449	0.459	0.457	0.504	0.474	0.488	0.483
Functional parameters	*Smr*	%	3.37	11.00	8.15	10.50	0.584	4.38	2.01	2.94
	Smc	µm	1.29	0.972	1.060	0.986	1.64	1.22	1.39	1.31
Spatial parameters	*Sal*	mm	0.0611	0.0656	0.0616	0.0611	0.0482	0.0511	0.0492	0.0489
	Str		0.311	0.334	0.125	0.127	0.305	0.319	0.307	0.309
	Std	°	56.3	56.3	56.3	56.3	109	109	109	109
Hybrid parameters	*Sdq*		0.0940	0.0534	0.0591	0.0599	0.1320	0.0692	0.0827	0.0788
	Sdr	%	0.441	0.143	0.175	0.180	0.868	0.239	0.342	0.310
Functional parameters (volume)	*Vm*	mm^3/mm^2	0.000024	0.000022	0.000027	0.000023	0.000025	0.000023	0.000024	0.000024
	Vv	mm^3/mm^2	0.000773	0.000722	0.000738	0.000733	0.000820	0.000775	0.000795	0.000787
	Vmp	mm^3/mm^2	0.000024	0.000022	0.000023	0.000023	0.000025	0.000023	0.000024	0.000024
	Vmc	mm^3/mm^2	0.000552	0.000520	0.000529	0.000528	0.000570	0.000536	0.000552	0.000546
	Vvc	mm^3/mm^2	0.000703	0.000657	0.000671	0.000666	0.000737	0.000697	0.000714	0.000707
	Vvv	mm^3/mm^2	0.000070	0.000064	0.000067	0.000067	0.000083	0.000079	0.000081	0.000081
Feature parameters	*Spd*	$1/mm^2$	1015	395	444	501	1415	392	581	614
	Spc	1/mm	0.0376	0.0195	0.0205	0.0229	0.0827	0.0312	0.042	0.0423
Functional parameters (stratified surfaces)	*Sk*	µm	1.59	1.50	1.52	1.53	1.62	1.51	1.55	1.55
	Spk	µm	0.435	0.403	0.413	0.411	0.467	0.439	0.450	0.442
	Svk	µm	0.610	0.551	0.578	0.567	0.766	0.716	0.757	0.751
	Sr1	%	7.88	7.92	7.84	7.62	8.76	8.89	8.77	8.57
	Sr2	%	89.6	89.9	89.7	89.7	88.8	88.6	88.7	88.7
Functional indices	*Sbi*		0.542	0.701	0.648	0.704	0.442	0.580	0.515	0.548
	Sci		1.48	1.49	1.48	1.48	1.45	1.45	1.44	1.45
	Svi		0.118	0.116	0.119	0.118	0.130	0.131	0.132	0.132

associated with the treatment orientation. Moreover, the TD function of NS filtered by SF did not contain so dominant direction over all of the directions and, generally, the graph demonstrated the most isotropic characteristics for this filtering technique. As the main limitation, all of the provided studies rely on precision in data analysis.

3.2. Improving the proposed profile validation method with direction and ISO 25178 roughness parameter variations analyses

The isotropy properties in the characterisation of the results of roughness metrology were found as critical in the analysis of the accuracy in both measurement and data study processes. When considering the effect of vibration on the mechanical performance results reliability, the high-frequency data must be studied comprehensively [91]. Vibration in the characterisation of machined parts can be classified as one of the main issues in reducing an accurate description of the measured data [92]. The correlation of vibration topography analysis to many surface data measurements and data studies was designated [93].

As defined previously, the high-frequency noisy data, characterised as noise surface, NS, must composed of the data from the required frequency or, at least, this frequency should be dominant. Additionally, those data should be isotropic so that the vibration of the measuring system influences the direction of the data equally. Therefore, the NS should be isotropic or the data included should include similar properties in each of the orientations. The direction properties of the data could be evaluated by an extraction of profile data from those areal. In Figs. 16 and 17, examples of milled composite or ceramic profile data were presented for NSs created by a GRF and SF application, respectively. Profiles were designated in three directions: horizontal, vertical and oblige according to the machining direction. For the results received after a GRF usage, the amplitude of the data, calculated as the total height of a raw profile *Pt*, varied significantly. Differences within milling for vertical or horizontal directions were 0.233 µm and 0.471 µm for composite and 0.147 µm and 0.371 µm for ceramic surfaces, respectively. In some examples, variations were higher than 100 %. One should stress, that significant improvement was achieved when an SF was employed. For milled surfaces, the Pt of profile varied from 0.461 µm to 0.495 µm and from 0.539 µm to 0.562 µm, correspondingly. Usually, the differences were smaller than 10 %.

The analysis of the profile data from the frequency domain exposed its similarity to the results received after the application of a selected type of filtering method in three directions. However, the profile data extracted from NSs obtained after the application of the SF consisted of high-frequency components more dominant after filtration by GRF. In Fig. 18, the spectral analysis calculated as PSD was verified and presented for each of the profiles extracted from NSs filtered from WLI-measured milled composite surfaces. Comparing two filters, GRF and SF, the ratio of high-frequency components was greater for all of the received frequencies when a spline method was accomplished. Further improvement in the NS characterisation was perceived when the shape of the ACF was considered. It was established, that the method of high-frequency noise suppression can be enhanced with an extensive characterisation of ACF calculated for the noisy data, NS in particular [94]. It was proved, that the increase of the high-frequency ratio from the whole noisy data caused an increase in the maximum value of the ACF. Practically, the more high-frequency data is dominant, the higher the ACF maximum value is. In Fig. 19, the profiles of ACF from NSs filtered from WLI-measured milled composite surfaces were presented in three

Table 2
The ISO 25178 roughness parameters of machined composite surfaces, evaluated for the raw measured data and those after noise removal by application of various methods.

Groups and parameters		Units	Honed composite				Milled composite			
			Raw measured	RGRF	SF	FFTF	Raw measured	RGRF	SF	FFTF
Height parameters	*Sq*	µm	0.425	0.365	0.397	0.389	0.790	0.760	0.777	0.772
	Ssk		−0.86	−0.97	−1.01	−1.02	−0.243	−0.227	−0.247	−0.243
	Sku		6.19	6.88	7.00	7.05	3.91	3.97	3.98	3.97
	Sp	µm	1.77	1.43	1.65	1.49	3.12	2.79	2.91	2.91
	Sv	µm	5.16	4.21	4.85	4.81	7.24	7.02	7.11	6.96
	Sz	µm	6.94	5.63	6.50	6.30	10.4	9.81	10.00	9.87
	Sa	µm	0.322	0.273	0.298	0.292	0.621	0.596	0.610	0.607
Functional parameters	*Smr*	%	1.94	9.34	2.94	7.48	0.237	0.789	0.528	0.516
	Smc	µm	1.28	1.01	1.20	1.05	2.11	1.83	1.93	1.93
Spatial parameters	*Sal*	mm	0.0156	0.0182	0.0156	0.0156	0.0702	0.0720	0.0713	0.0709
	Str		0.0402	0.0424	0.0384	0.0395	0.7630	0.7730	0.7660	0.7620
	Std	°	57.2	57.2	57.2	57.2	62.2	63.4	62.2	62.2
Hybrid parameters	*Sdq*		0.1300	0.0640	0.0849	0.0774	0.1220	0.0639	0.0796	0.0748
	Sdr	%	0.838	0.204	0.359	0.299	0.739	0.204	0.316	0.279
Functional parameters (volume)	*Vm*	mm^3/mm^2	0.000017	0.000014	0.000015	0.000015	0.000035	0.000034	0.000034	0.000034
	Vv	mm^3/mm^2	0.000512	0.000432	0.000469	0.000458	0.001040	0.001000	0.001020	0.001020
	Vmp	mm^3/mm^2	0.000017	0.000015	0.000015	0.000015	0.000035	0.000034	0.000034	0.000034
	Vmc	mm^3/mm^2	0.000353	0.000296	0.000324	0.000318	0.000692	0.000665	0.000681	0.000677
	Vvc	mm^3/mm^2	0.000450	0.000377	0.000409	0.000398	0.000943	0.000909	0.000928	0.000923
	Vvv	mm^3/mm^2	0.000062	0.000055	0.000060	0.000059	0.000096	0.000092	0.000094	0.000094
Feature parameters	*Spd*	$1/mm^2$	1077	308	445	401	217	79.9	117	113
	Spc	1/mm	0.0934	0.0323	0.0474	0.0396	0.0878	0.0267	0.0389	0.0350
Functional parameters (stratified surfaces)	*Sk*	µm	0.852	0.765	0.829	0.864	2.00	1.88	1.96	1.93
	Spk	µm	0.247	0.233	0.234	0.257	0.679	0.679	0.679	0.688
	Svk	µm	0.666	0.626	0.67	0.687	0.934	0.904	0.926	0.917
	Sr1	%	7.12	7.42	6.80	7.51	9.70	10.30	9.83	10.10
	Sr2	%	83.6	83.5	83.3	83.8	89.7	89.6	89.8	89.7
Functional indices	*Sbi*		0.369	0.405	0.367	0.416	0.429	0.487	0.469	0.465
	Sci		1.34	1.31	1.30	1.29	1.51	1.52	1.52	1.52
	Svi		0.146	0.151	0.151	0.152	0.122	0.121	0.122	0.121

directions of the extraction process. For the noisy data filtered by SF, the values of ACF increased more rapidly against those computed after a GRF. The description was highlighted by the arrows.

The selection of filter for high-frequency measurement noise reduction from the WLI measurement results was improved by studies of frequencies and heights of the profiles. Due to the homogenous requirement of the noisy data, profiles extracted from NS should be similar due to frequencies and heights. The maximum heights of the profiles extracted from NS filtered by the spline method were the most similar against Gaussian (regular or robust), morphological or Fourier filtering techniques as reported for the composite or ceramic surfaces after the machining process.

Studying the variations in ISO 25178 roughness parameters when applying noise-removal techniques, the variations of noise-sensitive parameters were considered. It was evaluated, that the occurrence of high-frequency noise impacts selected roughness parameters much more than others [95]. The hybrid *Sdq* and *Sdr*, feature *Spc* and *Spd* [62] and functional *Smr* and *Sk* [36] indicators were classified as especially vulnerable to the presence of high-frequency measurement errors. Those roughness parameters were classified as noise-sensitive.

According to the noise-suppression filters proposed in the study, the values of both groups' parameters varied from the values calculated for the raw measured topography data. In Tables 1 and 2, the values of ISO 25178 roughness parameters were presented for ceramic and composite surface data filtered by GRF, SF and FFTF techniques.

Variations in the parameters characterising the peaks, including curvature *Spc* and density *Spd*, were obvious and retrieved around more than 100 % of deviations. Values of those indicators decreased for both types of surfaces. The areal material ratio *Smr* increased for both types of machined surfaces but the RGRF method provides the largest variations. The hybrid *Sdq* parameter decreased by around 30–50 % for the ceramic machined surfaces and these variations were also smaller after the application of SF and FFTF techniques contrary to the RGRF method.

Considering the variations of non-noise parameters, the most promising results were obtained for the SF applications. The non-noise parameters were those of ISO 25178 indicators whose values were not significantly modified when noise-suppression filters were applied. The values of amplitude parameters were modified usually by less than 10 % when for most of them variations were smaller than 5 % for the results collected after an SF application to the machined composite surfaces. As for previous characterisations, the variations in non-noise parameters were enlarged after the application of the RGRF technique contrary to the SF and FFTF approaches but, statistically, distortions in non-noise parameters were minimised with the spline filtering procedure.

Distortion of the Sdq parameter, related to the slope of the surface and more correlated with amplitude than a surface wavelength, considering the random surfaces, its variations are associated with the Sq indicator. Since both hybrid parameters, Sdq and Sdr, are interconnected, the correlation between them is extremely high. Further, amplitude parameters are strongly related to many machined surface performances.

It was found that the amplitude skewness Ssk and kurtosis Sku indicators were crucial in identifying surfaces after different machining processes [96]. The burnishing parameters were also addressed as correlated to both ISO 25178 height parameters [97].

The proposed methodology for the selection of the filter and its

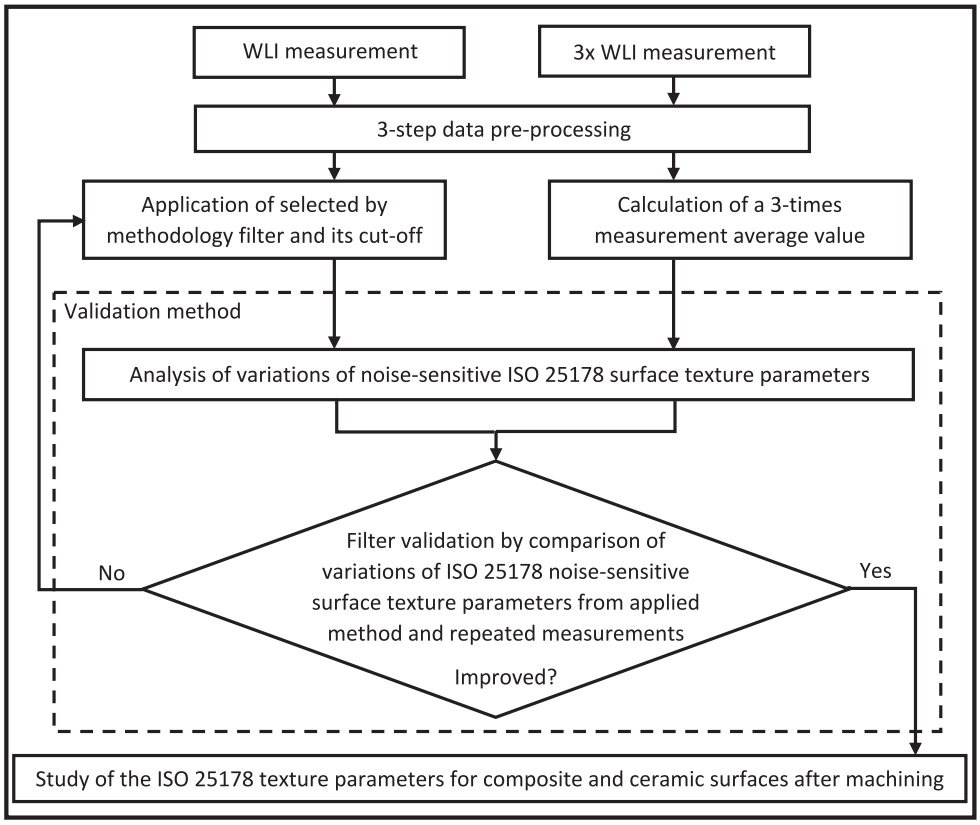

Fig. 20. The flow chart of the validation procedure for the proposed methodology.

bandwidth was validated by comparing it to the repeated measurement at the same conditions. The variations of noise-sensitive ISO 25178 texture parameters calculated for the data before and after filtration defined by the proposed approach were compared to the differences of noise-sensitive parameters computed from three measurements. The variations in results received by 7.5 μm spline filtering were the most similar to the variations from repeated measurements. The flow chart of the applied validation method is presented in Fig. 20.

Generally, the proposed procedure was found promising in the process of selection of a filter with a cut-off for the reduction of the influence of the high-frequency measurement noise for the evaluation of composite or ceramic surface topography after the machining process.

As the final results presented, the high-frequency measurement noise, whose origin is usually from the vibration of the measuring system, can significantly affect the final measurement results from the surface topography data. Application of the noise-separation data processing technique seems to be essential as a comprehensive analysis of the machining process.

The proposed approach can be studied for various types of contactless surface topography measuring instruments and surfaces after different manufacturing processes. Since the general surface data analysis functions are not limited to the type of topography, further studies can be addressed to both different types of manufactured materials and measuring instruments.

4. Conclusions

Based on the studies presented, the following conclusions were drawn as follows:

1. The vibration of the surface topography measuring system can cause the enlargement of errors in the evaluation of ISO 25178 roughness parameters. A comprehensive study of variations of roughness indicators enabled to classification of selected topography parameters into those susceptible to the presence of high-frequency measurement noise, e.g. the hybrid *Sdq* and *Sdr*, feature *Spc* and *Spd* and functional *Smr* and *Sk*.
2. For the selection of a filter with a cut-off dedicated to the minimisation of high-frequency measurement errors, a proposed procedure with a comprehensive study of noisy data, defined as the data removed by a noise-suppression filter, could be exceedingly valuable. However, the raw measured data decomposition process must be verified adequately.
3. The effect of noise filtering with a method based on the profile direction analysis studied during the analysis of machined composite or ceramic surfaces was compared. It was verified, that the results can be improved with a proposed method when the isotropy characteristics of the noisy data are considered.
4. The application of SF provided the most encouraging effects for the removal of high-frequency measurement noise for machined composite or ceramic surface topography measurement results. This type of data filtering technique can be appropriate in a high-frequency error reduction for various types of machined composite or ceramic surfaces.
5. When verifying the proposed procedure, the variations of ISO 25178 roughness parameters were studied. It was assumed, that the spline filtering method with a 7.5 μm cut-off value applied against commonly used filtering techniques including regular Gaussian isotropic, robustly modified Gaussian, morphological and Fourier filters, caused the smallest distortions in surface topography parameters.
6. Finally, when reducing the distortions in an evaluation of ISO 25178 roughness parameters, often caused by the vibrational high-frequency measurement noise, multithreaded characterisation is required. Firstly, the removed noisy data must be consisted of the high-frequency components. Secondly, it must be isotropic. Such

validation can improve a profile direction method, however, considering the profile's noisy data, the high-frequency components must be dominant.

7. A fast and precise surface topography high-frequency measurement noise reduction approach is significant in industrial applications that can minimise the time-consuming procedure based on measurement repetition. Additionally, due to the common data processing techniques, where the measurement process is iterated at least three times, the proposed scheme can be especially valuable in the control time.

CRediT authorship contribution statement

Przemysław Podulka: Writing – original draft, Visualization, Validation, Software, Resources, Methodology, Investigation, Formal analysis, Data curation, Conceptualization. **Wojciech Macek:** Writing – review & editing, Visualization, Supervision, Software, Resources, Formal analysis, Data curation. **Mirosław Szala:** Writing – review & editing, Validation, Supervision, Formal analysis, Data curation. **Andrzej Kubit:** Writing – review & editing, Visualization, Supervision, Formal analysis, Data curation. **Kinkar Chandra Das:** Writing – review & editing, Validation, Supervision. **Grzegorz Królczyk:** Writing – review & editing, Validation, Supervision.

Declaration of competing interest

The authors declare that they have no known competing financial interests or personal relationships that could have appeared to influence the work reported in this paper.

References

[1] Wang P, Liang H, Jiang L, Qian L. Effect of nanoscale surface roughness on sliding friction and wear in mixed lubrication. Wear 2023;530–531:204995. https://doi.org/10.1016/j.wear.2023.204995.

[2] Sherrington I, Smith EH. The significance of surface topography in engineering. Precis Eng 1986;8(2):79–87. https://doi.org/10.1016/0141-6359(86)90090-5.

[3] Chowdhury SKR, Kaliszer H, Rowe GW. An analysis of changes in surface topography during running-in of plain bearings. Wear 1979;57(2):331–43. https://doi.org/10.1016/0043-1648(79)90107-8.

[4] Leksycki K, Maruda RW, Feldshtein E, Wojciechowski S, Habrat W, Gupta MK, et al. Evaluation of tribological interactions and machinability of Ti6Al4V alloy during finish turning under different cooling conditions. Tribology International 2023;189:109002. https://doi.org/10.1016/j.triboint.2023.109002.

[5] Lee WB, Cheung CF. A dynamic surface topography model for the prediction of nano-surface generation in ultra-precision machining. International Journal of Mechanical Sciences 2001;43(4):961–91. https://doi.org/10.1016/S0020-7403(00)00050-3.

[6] Waikar RA, Guo YB. A comprehensive characterization of 3D surface topography induced by hard turning versus grinding. J Mater Process Technol 2008;197(1–3):189–99. https://doi.org/10.1016/j.jmatprotec.2007.05.054.

[7] Wojciechowski Ł, Gapiński B, Firlik B, Mathia TG. Characteristics of tram wheel wear: focus on mechanism identification and surface topography. Tribology International 2020;150:106365. https://doi.org/10.1016/j.triboint.2020.106365.

[8] Song J, Chu W, Vorburger TV, Thompson R, Renegar TB, Zheng A, et al. Development of ballistics identification-from image comparison to topography measurement in surface metrology. Measurement Science and Technology 2012;23(5):054010. https://doi.org/10.1088/0957-0233/23/5/054010.

[9] Benardos PG, Vosniakos GC. Predicting surface roughness in machining: a review. Int J Mach Tool Manuf 2003;43(8):833–44. https://doi.org/10.1016/S0890-6955(03)00059-2.

[10] Szwajka K, Zielińska-Szwajka J, Trzepieciński T. The use of a radial basis function neural network and fuzzy modelling in the assessment of surface roughness in the MDF milling process. Materials 2023;16:5292. https://doi.org/10.3390/ma16155292.

[11] Asakura T. Surface roughness measurements. In: Erf RK, editor. Speckle Metrology. New York: Academic Press; 1978. p. 11–49.

[12] Vorburger TV, Rhee H-G, Renegar TB, Song J-F, Zheng A. Comparison of optical and stylus methods for measurement of surface texture. The International Journal of Advanced Manufacturing Technology 2007;33:110–8. https://doi.org/10.1007/s00170-007-0953-8.

[13] Bai J, Li X, Wang X, Wang J, Ni K, Zhou Q. Self-reference dispersion correction for chromatic confocal displacement measurement. Opt Lasers Eng 2021;140:106540. https://doi.org/10.1016/j.optlaseng.2021.106540.

[14] Shahabi HH, Ratnam MM. Noncontact roughness measurement of turned parts using machine vision. The International Journal of Advanced Manufacturing Technology 2010;46:275–84. https://doi.org/10.1007/s00170-009-2101-0.

[15] Dresel T, Häusler G, Venzke H. Three-dimensional sensing of rough surfaces by coherence radar. Appl Optics 1992;31(7):919–25. https://doi.org/10.1364/AO.31.000919.

[16] Dong Y, Li Z, Zhu L, Zhang X. Topography measurement and reconstruction of inner surfaces based on white light interference. Measurement 2021;186:110199. https://doi.org/10.1016/j.measurement.2021.110199.

[17] Viotti MR, Albertazzi A, Fantin AV, Dal Pont A. Comparison between a white-light interferometer and a tactile formtester for the measurement of long inner cylindrical surfaces. Opt Lasers Eng 2008;46(5):396–403. https://doi.org/10.1016/j.optlaseng.2007.12.004.

[18] Wu X, Zhu L, Fang F, Zhang X. Research on the quality control technology of micro-topography machining based on in situ white light interferometry. Measurement 2023;220:113257. https://doi.org/10.1016/j.measurement.2023.113257.

[19] Li D, Tong Z, Jiang X, Blunt L, Gao F. Calibration of an interferometric on-machine probing system on an ultra-precision turning machine. Measurement 2018;118:96–104. https://doi.org/10.1016/j.measurement.2017.12.038.

[20] Podulka P, Pawlus P, Dobrzański P, Lenart A. Spikes removal in surface measurement. J Phys Conf Ser 2014;483:012025. https://doi.org/10.1088/1742-6596/483/1/012025.

[21] Pawlus P, Reizer R, Wieczorowski M. Comparison of results of surface texture measurement obtained with stylus methods and optical methods. Metrology and Measurement Systems 2018;25:589–602. https://doi.org/10.24425/123894.

[22] De Lega CX, De Groot PJ. Characterization of materials and film stacks for accurate surface topography measurement using a white-light optical profiler. In: ; 2008. https://doi.org/10.1117/12.782836. 69950P.

[23] Zhen L, Gröger S. Experimental study of non-measured points on surface measurement using structured illumination microscopy. Metrology and Measurement Systems 2022;29(4):763–78. https://doi.org/10.24425/mms.2022.143071.

[24] Pawlus P, Reizer R, Wieczorowski M. Problem on non-measured points in surface texture measurements. Metrology and Measurement Systems 2017;24:525–36. https://doi.org/10.1515/mms-2017-0046.

[25] Waikar RA, Guo YB. A comprehensive characterization of 3D surface topography induced by hard turning versus grinding. J Mater Process Technol 2008;197(1–3):189–99. https://doi.org/10.1016/j.jmatprotec.2007.05.054.

[26] Ismail FM, Yanagi K, Fujii A. An outlier correction procedure and its application to areal surface data measured by optical instruments. Measurement Science and Technology 2010;21:105105. https://doi.org/10.1088/0957-0233/21/10/105105.

[27] Podulka P. The effect of spikes occurrence on surface texture parameter assessments. IOP Conf Ser: Mater Sci Eng 2019;473(1):012039. https://doi.org/10.1088/1757-899X/473/1/012039.

[28] Wang C, Caja J, Gómez E. Comparison of methods for outlier identification in surface characterization. Measurement 2018;117:312–25. https://doi.org/10.1016/j.measurement.2017.12.015.

[29] Le Goic G, Brown CA, Favreliere H, Samper S, Formosa F. Outlier filtering: a new method for improving the quality of surface measurements. Measurement Science and Technology 2012;24:015001. https://doi.org/10.1088/0957-0233/24/1/015001.

[30] Maculotti G, Genta G, Quagliotti D, Galetto M, Hansen HN. Gaussian process regression-based detection and correction of disturbances in surface topography measurements. Quality and Reliability Engineering International 2022;38:1501–18. https://doi.org/10.1002/qre.2980.

[31] ISO 2016 25178-600. *Geometrical Product Specification (GPS)—Surface Texture: Areal Part 600: Metrological Characteristics for Areal-Topography Measuring Methods*; International Organization for Standardization: Geneva, Switzerland, 2016.

[32] Zuo X, Peng M, Zhou Y. Influence of noise on the fractal dimension of measured surface topography. Measurement 2020;152:107311. https://doi.org/10.1016/j.measurement.2019.107311.

[33] De Groot P, DiSciacca J. Definition and evaluation of topography measurement noise in optical instruments. Optical Engineering 2020;59:064110. https://doi.org/10.1117/1.OE.59.6.064110.

[34] Gomez C, Su R, de Groot P, Leach RK. Noise reduction in coherence scanning interferometry for surface topography measurement. Nanomanufacturing and Metrology 2020;3:68–76. https://doi.org/10.1007/s41871-020-00057-4.

[35] Vanrusselt M, Haitjema H, Leach RK, de Groot P. International comparison of noise in areal surface topography measurements. Surface Topography: Metrology and Properties 2021;9:025015. https://doi.org/10.1088/2051-672X/abfa29.

[36] Podulka P. Reduction of influence of the high-frequency noise on the results of surface topography measurements. Materials 2021;14:333. https://doi.org/10.3390/ma14020333.

[37] Podulka P, Macek W, Branco R, Nejad RM. Reduction in errors in roughness evaluation with an accurate definition of the S-L surface. Materials 1865;2023:16. https://doi.org/10.3390/ma16051865.

[38] Podulka P. Detection of measurement noise in surface topography analysis. J Phys: Conf Ser 2021;1736:012014. https://doi.org/10.1088/1742-6596/1736/1/012014.

[39] Sun J, Song Z, Heb G, Sang Y. An improved signal determination method on machined surface topography. Precis Eng 2018;51:338–47. https://doi.org/10.1016/j.precisioneng.2017.09.004.

[40] Jacobs TDB, Junge T, Pastewka L. Quantitative characterization of surface topography using spectral analysis. Surface Topography: Metrology and Properties 2017;5:013001. https://doi.org/10.1088/2051-672X/aa51f8.

[41] Syam WP. In-process surface topography measurements. Bristol, UK: Advances in Optical Surface Texture Metrology Leach RK. Ed. IOP Publishing; 2020.
[42] Podulka P. Proposals of frequency-based and direction methods to reduce the influence of surface topography measurement errors. Coatings 2022;12:726. https://doi.org/10.3390/coatings12060726.
[43] Dzierwa A, Reizer R, Pawlus P, Grabon W. Variability of areal surface topography parameters due to the change in surface orientation to measurement direction. Scanning 2014;36:170–83. https://doi.org/10.1002/sca.21115.
[44] Chen S, Zhao W, Yan P, Qiu T, Gu H, Jiao L, et al. Effect of milling surface topography and texture direction on fatigue behavior of ZK61M magnesium alloy. International Journal of Fatigue 2022;156:106669. https://doi.org/10.1016/j.ijfatigue.2021.106669.
[45] Macek W, Branco R, Podulka P, Kopec M, Zhu SP, Costa JD. A brief note on entire fracture surface topography parameters for 18Ni300 maraging steel produced by LB-PBF after LCF. Engineering Failure Analysis 2023;153:107541. https://doi.org/10.1016/j.engfailanal.2023.107541.
[46] Macek W, Rozumek D, Faszynka S, Branco R, Zhu SP, Nejad RM. Fractographic-fractal dimension correlation with crack initiation and fatigue life for notched aluminium alloys under bending load. Engineering Failure Analysis 2023;149:107285. https://doi.org/10.1016/j.engfailanal.2023.107285.
[47] Macek R, Branco R, Podulka P, Nejad RM, Costa JD, Ferreira JAM, et al. The correlation of fractal dimension to fracture surface slope for fatigue crack initiation analysis under bending-torsion loading in high-strength steels. Measurement 2023;218:113169. https://doi.org/10.1016/j.measurement.2023.113169.
[48] Zhang B, Lu S, Rabiey M, Axinte D, Bleicher F. Grinding of composite materials. CIRP Annals 2023;72(2):645–71. https://doi.org/10.1016/j.cirp.2023.05.001.
[49] Adibi H, Esmaeili H, Rezaei SM. Study on minimum quantity lubrication (MQL) in grinding of carbon fiber-reinforced SiC matrix composites (CMCs). The International Journal of Advanced Manufacturing Technology 2018;95:3753–67. https://doi.org/10.1007/s00170-017-1464-x.
[50] Blau PJ, Jolly BC. Relationships between abrasive wear, hardness, and grinding characteristics of titanium-based metal-matrix composites. Journal of Materials Engineering and Performance 2009;18:424–32. https://doi.org/10.1007/s11665-008-9227-3.
[51] Cao X, Lin B, Zhang X. Investigations on grinding process of woven ceramic matrix composite based on reinforced fiber orientations. Compos Part B Eng 2015;71:184–92. https://doi.org/10.1016/j.compositesb.2014.11.029.
[52] Du J, Ming W, Ma J, He W, Cao Y, Li X, et al. New observations of the fiber orientations effect on machinability in grinding of C/SiC ceramic matrix composite. Ceram Int 2018;44(12):13916–28. https://doi.org/10.1016/j.ceramint.2018.04.240.
[53] Zhu C, Gu P, Wu Y, Liu D, Wang X. Surface roughness prediction model of SiCp/Al composite in grinding. International Journal of Mechanical Sciences 2019;155:98–109. https://doi.org/10.1016/j.ijmecsci.2019.02.025.
[54] Azmir MA, Ahsan AK. Investigation on glass/epoxy composite surfaces machined by abrasive water jet machining. J Mater Process Technol 2008;198(1–3):122–8. https://doi.org/10.1016/j.jmatprotec.2007.07.014.
[55] Samant AN, Dahotre NB. Laser machining of structural ceramics—a review. J Eur Ceram Soc 2009;29(6):969–93. https://doi.org/10.1016/j.jeurceramsoc.2008.11.010.
[56] An Q, Chen J, Ming W, Chen M. Machining of SiC ceramic matrix composites: a review. Chin J Aeronaut 2021;34(4):540–67. https://doi.org/10.1016/j.cja.2020.08.001.
[57] Diaz OG, Luna GG, Liao Z, Axinte D. The new challenges of machining ceramic matrix composites (CMCs): review of surface integrity. Int J Mach Tool Manuf 2019;139:24–36. https://doi.org/10.1016/j.ijmachtools.2019.01.003.
[58] Pawlus P, Reizer R, Krolczyk GM. Modelling and prediction of surface textures after abrasive machining processes: a review. Measurement 2023;220:113337. https://doi.org/10.1016/j.measurement.2023.113337.
[59] Singh RP, Singhal S. Investigation of machining characteristics in rotary ultrasonic machining of alumina ceramic. Materials and Manufacturing Processes 2017;32(3):309–26. https://doi.org/10.1080/10426914.2016.1176190.
[60] Pawlus P, Reizer R, Wieczorowski M, Grzegorz Królczyk G. Parametric description of one-process surface texture. Measurement 2022;204:112066. https://doi.org/10.1016/j.measurement.2022.112066.
[61] Whitehouse DJ. Handbook of surface and Nanometrology. Taylor & Francis Group, Boca Raton: CRC Press; 2011.
[62] Pawlus P, Reizer R, Wieczorowski M, Krolczyk GM. Study of surface texture measurement errors. Measurement 2023;210:112568. https://doi.org/10.1016/j.measurement.2023.112568.
[63] Agarwal S, Rao PV. Modeling and prediction of surface roughness in ceramic grinding. Int J Mach Tool Manuf 2010;50(12):1065–76. https://doi.org/10.1016/j.ijmachtools.2010.08.009.
[64] ISO 25178-2:2021; *Geometrical product specifications (GPS) — Surface texture: Areal — Part 2: Terms, definitions and surface texture parameters*. ISO: Geneva, Switzerland, 2021.
[65] ISO 16610-61:2015. *Geometrical Product Specification (GPS)—Filtration—Part 61: Linear Areal Filters—Gaussian Filters*; ISO: Geneva, Switzerland, 2015.
[66] ISO 16610-71:2014. *Geometrical product specifications (GPS) — Filtration — Part 71: Robust areal filters: Gaussian regression filters*; ISO: Geneva, Switzerland, 2014.
[67] ISO 16610-62:2023. *Geometrical product specifications (GPS) — Filtration — Part 62: Linear areal filters: spline filters*; ISO: Geneva, Switzerland, 2023.
[68] ISO 16610-85:2013. Geometrical product specifications (GPS) — Filtration — Part 85: Morphological areal filters: Segmentation; ISO: Geneva, Switzerland, 2013.
[69] Podulka P. Feature-based characterisation of turned surface topography with suppression of high-frequency measurement errors. Sensors 2022;22:9622. https://doi.org/10.3390/s22249622.
[70] Podulka P. Thresholding methods for reduction in data processing errors in the laser-textured surface topography measurements. Materials 2022;15:5137. https://doi.org/10.3390/ma15155137.
[71] Pawlus P, Reizer R, Wieczorowski M, Krolczyk GK. Sensitivities of surface texture parameters to measurement errors – a review. Measurement 2024;227:114323. https://doi.org/10.1016/j.measurement.2024.114323.
[72] ISO 25178-700:2022. Geometrical product specifications (GPS) Surface texture: Areal Part 700: Calibration, adjustment and verification of areal topography measuring instruments. Geneva, Switzerland: International Organization for Standardization; 2022.
[73] Shao Y, Xu F, Chen J, Lu J, Du S. Engineering surface topography analysis using an extended discrete modal decomposition. Journal of Manufacturing Processes 2023;90:367–90. https://doi.org/10.1016/j.jmapro.2023.02.005.
[74] Hanada H, Saito T, Hasegawa M, Yanagi K. Sophisticated filtration technique for 3D surface topography data of rectangular area. Wear 2008;264(5–6):422–7. https://doi.org/10.1016/j.wear.2006.08.035.
[75] Brinkman S, Bodschwinna H. Advanced Gaussian filters. In: Blunt L, Jiang X, editors. Assessment surface topography. Kogan Page Science: London and Sterling; 2003. p. 62–89.
[76] Podulka P. Improved procedures for feature-based suppression of surface texture high-frequency measurement errors in the wear analysis of cylinder liner topographies. Metals 2021;11:143. https://doi.org/10.3390/met11010143.
[77] Podulka P, Macek W, Zima B, Lesiuk G, Branco R, Królczyk G. Roughness evaluation of turned composite surfaces by analysis of the shape of autocorrelation function. Measurement 2023;222:113640. https://doi.org/10.1016/j.measurement.2023.113640.
[78] Jiang X, Senin N, Scott PJ, Blateyron F. Feature-based characterisation of surface topography and its application. CIRP Annals 2021;70(2):681–702. https://doi.org/10.1016/j.cirp.2021.05.001.
[79] Guo MX, Liu J, Pan LM, Wu CJ, Jiang XH, Guo WC. An integrated machine-process-controller model to predict milling surface topography considering vibration suppression. Advances in Manufacturing 2020;10:443–58. https://doi.org/10.1007/s40436-021-00386-7.
[80] Janecki D. Edge effect elimination in the recursive implementation of Gaussian filters. Precis Eng 2012;36:128–36. https://doi.org/10.1016/j.precisioneng.2011.08.001.
[81] Janecki D. A generalized L2-spline filter. Measurement 2009;42:937–43. https://doi.org/10.1016/j.measurement.2009.01.020.
[82] Lou S, Jiang X, Scott PJ. Application of the morphological alpha shape method to the extraction of topographical features from engineering surfaces. Measurement 2013;46:1002–8. https://doi.org/10.1016/j.measurement.2012.09.015.
[83] Podulka P. Comparisons of envelope morphological filtering methods and various regular algorithms for surface texture analysis. Metrology and Measurement Systems 2020;27:243–63. https://doi.org/10.24425/mms.2020.132772.
[84] Zakharov OV, Ivanova TN, Pugin KG. Variable asymmetric morphological profile filter for roughness analysis. *6th scientific school dynamics of complex networks and their applications (DCNA)*. Kaliningrad, Russian Federation 2022:312–5. https://doi.org/10.1109/DCNA56428.2022.9923149.
[85] Tien CL, Yang HM, Liu MC. The measurement of surface roughness of optical thin films based on fast Fourier transform. Thin Solid Films 2009;517(17):5110–5. https://doi.org/10.1016/j.tsf.2009.03.193.
[86] Macek W. The impact of surface slope and calculation resolution on the fractal dimension for fractures of steels after bending-torsion fatigue. Surface Topography: Metrology and Properties 2022;10:015030. https://doi.org/10.1088/2051-672X/AC58AE.
[87] Podulka P. Fast Fourier transform detection and reduction of high-frequency errors from the results of surface topography profile measurements of honed textures. Eksploatacja i Niezawodność – Maintenance and Reliability 2021;23:84–93. https://doi.org/10.17531/ein.2021.1.9.
[88] Blateyron F. The areal field parameters. In: Leach, R.K. *Characterisation of areal surface texture*. Springer; 2013. p. 15–43.
[89] Podulka P. The effect of surface topography feature size density and distribution on the results of a data processing and parameters calculation with a comparison of regular methods. Materials 2021;14:4077. https://doi.org/10.3390/ma14154077.
[90] Podulka P. Suppression of the high-frequency errors in surface topography measurements based on comparison of various spline filtering methods. Materials 2021;14:5096. https://doi.org/10.3390/ma14175096.
[91] Tandon N, Choudhury A. A review of vibration and acoustic measurement methods for the detection of defects in rolling element bearings. Tribology International 1999;32(8):469–80. https://doi.org/10.1016/S0301-679X(99)00077-8.
[92] Cai C, An Q, Chen M, Ming W. Modelling of end-milled floor surface topography considering system vibration and tool deflection. J Mater Process Technol 2023;312:117864. https://doi.org/10.1016/j.jmatprotec.2023.117864.
[93] Macek W, Marciniak Z, Branco R, Rozumek D, Królczyk GM. A fractographic study exploring the fracture surface topography of S355J2 steel after pseudo-random bending-torsion fatigue tests. Measurement 2021;178:109443. https://doi.org/10.1016/j.measurement.2021.109443.
[94] Podulka P. Resolving selected problems in surface topography analysis by application of the autocorrelation function. Coatings 2023;13:74. https://doi.org/10.3390/coatings13010074.

[95] Podulka P. Roughness evaluation of burnished topography with a precise definition of the S-L surface. Applied Sciences 2022;12:12788. https://doi.org/10.3390/app122412788.
[96] Krolczyk GM, Krolczyk JB, Maruda RW, Legutko S, Tomaszewski M. Metrological changes in surface morphology of high-strength steels in manufacturing processes. Measurement 2016;88:176–85. https://doi.org/10.1016/j.measurement.2016.03.055.
[97] Świrad S, Wydrzynski D, Niesłony P, Krolczyk GM. Influence of hydrostatic burnishing strategy on the surface topography of martensitic steel. Measurement 2019;138:590–601. https://doi.org/10.1016/j.measurement.2019.02.081.